

The effects of pollution on CO₂ exchange in a Boreal Forest

Yichu Chen

A Thesis submitted to the Faculty of Graduate Studies
in Partial Fulfillment of the Requirements for the
Degree of Master of Science

Graduate Program in Earth and Space Science

York University

Toronto, Ontario

February 2022

Abstract

Boreal forests are the largest biological community on earth, with an area of about 14.7×10^6 km². Canada has about 270 Mha of boreal forests. The carbon balance and carbon absorption of Canadian boreal forests will affect the global atmospheric carbon budget and the global stability of carbon dioxide. CO₂ exchanges were studied through the analysis of temperature, H₂O, CO₂ concentration and CO₂ flux. The purpose of this project is to analyze the CO₂ exchange at the York Athabasca Jack Pine (YAJP) site near oil sands facilities. The results show that both temperature and water vapour affected the CO₂ concentration and flux. When the wind direction was 170° to 190°, a higher concentration of pollutants was measured at the YAJP site. The CO₂ concentration during pollution episodes was 17.3 (1.6) mmol/m³ and the CO₂ flux was -5.5 (1.4) μmol/m²/s. These values are compared to 16.8 (0.6) mmol/m³ and -3.4 (0.2) μmol/m²/s when winds were not from this range (numbers in brackets are the standard deviations). These results suggest that pollution from the Alberta oil sands processing facility affects the exchange of CO₂ to and from the boreal forest.

Content

Abstract	ii
List of Figures	v
List of Table	viii
1. Introduction	1
1.1 Boreal Forest in Canada.....	3
2. Background	6
2.1 Related work	6
2.1.1 The exchange of carbon dioxide between vegetation and the atmosphere ..	6
2.1.2 CO ₂ in the Boreal Forest	8
2.1.3 Pollution released by oil sands region.	10
2.1.4 Turbulent fluxes and spectra	11
2.1.5 Research tasks	12
2.2 CO ₂ fluxes of different forests	13
2.3 The impact of different vegetation on CO ₂ changes (forest, moss, lichen)	17
2.4 Changes in the CO ₂ flux of the forest after fire	18
2.5 Modeling of CO ₂ fluxes.....	19
3. Method	21
3.1 Study Site description	21
3.2 Study Site selection.....	24
3.3 YAJP tower and Instrumentation	26
3.3.1 Sonic anemometers	28
3.3.2 Light sensors	29
3.3.3 CO ₂ /H ₂ O gas analyzers	29
3.3.4 Thermo Scientific model 43i	30
3.4 CO ₂ Eddy Covariance Measurement	30
3.4.1 Removal of outliers.....	31
3.4.2 Coordinate rotation	32
3.5 Data measurement.....	34
3.6 Selection for Yearly Comparisons.....	36
3.7 Analysis Methodology	37
4. Result	39
4.1 Energy spectra.....	39
4.2 Monthly average	40
4.3 Wind Direction Description	42
4.4 Analysis of Temperature from Sonic anemometer.....	43
4.5 Analysis of water vapour	45
4.6 CO ₂ concentration.....	47
4.7 CO ₂ flux	50
4.8 Photosynthetically Active Radiation (PAR).....	53
4.9 CO ₂ flux calculated by the CLM model	54

4.10 CO ₂ concentration and SO ₂ concentration with wind direction.....	55
5. Discussion.....	58
5.1 Comparison of temperature, water vapour concentration, PAR, CO ₂ concentration and CO ₂ flux	58
5.2 Comparison of the CO ₂ flux calculated by the CLM5.0 model and the CO ₂ flux of this project.....	63
5.3 Comparison of CO ₂ concentration with other studies.....	64
5.4 Comparisons of CO ₂ flux with other studies	66
6. Conclusion	69
References	71

List of Figures

Figure 1.1: Kurz et al. (2013). Geographic relationship between the boreal zone as defined by Brandt (2009), the managed forest as defined by Canada for the purposes of reporting to the UNFCCC (Stinson et al. 2011), and permafrost zones (Hegginbottom et al. 1995). The orange area is Alberta where the study area is located. The red dot is the Athabasca oil sands region.	4
Figure 2.1: Juurola et al. (2016). Changes in light, temperature and photosynthesis of plants throughout the year at Hyytiälä Forestry Field Station located in Juupajoki, Southern-Finland.	8
Figure 2.2: Eija Juurola et al. (2016). The capture and release of carbon dioxide (CO ₂) by the forest.....	9
Figure 2.3: Baldocchi et al. (1997). A typical diurnal course of net ecosystem exchange (NEE) of CO, and the flux (F _C) associated with the storage (F _{storage}) of CO, in the underlying air layer.....	10
Figure 2.4: Foken et al. (2008). Schematic plot of the turbulence spectra and the ranges of energy production (A), the inertial sub-range (B) and the dissipation range (C) dependent on the wave number k (Kaimal and Finnigan 1994).....	12
Figure 2.5: Froelich et al. (2015). Annual totals of gross ecosystem productivity (GEP), ecosystem respiration (RE), and net ecosystem productivity (NEP).	16
Figure 2.6: Mammarella et al. (2007). Mean diurnal course of CO ₂ fluxes with standard error bars for the summer 2004 in Hyytiälä Forest.	17
Figure 2.7: Köster et al. (2018). Average carbon dioxide (CO ₂) flux (µg CO ₂ m ⁻² s ⁻¹) (n=72 per measurement period) per analyzed fire age class. Vertical bars represent the standard errors.	19
Figure 3.1: From Jiang (2018). Boreal forest crown in the vicinity of the YAJP tower. Photo taken July 2017.	22
Figure 3.2: (a) The orange area is the location of the study area. (b) The grey spot indicates the YAJP tower site. The blue polygonal area is the Syncrude processing facility, the yellow polygonal area is the Suncor processing facility, the purple polygonal area is the Shell Albian processing facility, and the red polygonal area is the CNRL processing facility..	23
Figure 3.3: From Jiang (2018). Emission sources in the oil sands area. Purple polygons indicate emission sources. Orange polygons indicate possible sources which emit low amounts of particulates. These were determined by the emissions inventory in (ECCC 2016) and analysis from the WBEA data. Blue pointers indicate WBEA towers used in the Jiang (2018) analysis. Blue pointer with a white circle around it is AMS 13. Black lines delimit angles with elevated particulate concentrations; such angles lay in the sector with an arc.	25
Figure 3.4: Schematic sketch of instrumentation placement on tower. Not to scale.	28
Figure 3.5: An example of raw CO ₂ concentration data, with outliers.	32
Figure 3.6: A sample of clean data (outliers removed).	32

Figure 3.7: Wilczak et al. (2008). Definition of the coordinate rotations: (a) first rotation; (b) second rotation.	33
Figure 3.8: Raw data of CO ₂ concentration (red dots) and data with outliers removed of CO ₂ concentration (black dots) from August 2017 to August 2021.	34
Figure 3.9: Raw data of CO ₂ flux (red dots) and data with outliers removed of CO ₂ flux (black dots) from August 2017 to August 2021.	35
Figure 3.10: Data of SO ₂ concentration from June 10th to 17th, 2018.	35
Figure 4.1: CO ₂ flux spectrum at a height of 31 m in 2018.	39
Figure 4.2: The average CO ₂ concentration for each month from 2017, 2018, 2019, 2020, and 2021.	41
Figure 4.3: The average CO ₂ flux for each month with standard deviations from 2017, 2018, 2019, 2020, and 2021.	41
Figure 4.4: The relationship between wind direction and wind speed (m/s) at the height of 31m from 2017 to 2021.	42
Figure 4.5: Temperature data from Sonic anemometer s at 31 m (High) and 5 m (Low). (a): temperature data in 2018. (b): temperature data in 2019. (c): temperature data in 2020. (d): temperature data in 2021. The temperature data at a height of 5 meters was not recorded in March and April 2019 and 2021. Data were measured by YAJP tower.	44
Figure 4.6: (a): H ₂ O data in 2018. (b): H ₂ O data in 2019. c): H ₂ O data in 2020. (d): H ₂ O data in 2021. Data were measured by YAJP tower.	46
Figure 4.7.1: The relationship between CO ₂ concentration (red lines) and temperature (black line) and water concentration (blue line) in 2018. Data were measured by YAJP tower.	48
Figure 4.7.2: As Figure 4.7.1 for 2019.	48
Figure 4.7.3: As Figure 4.7.1 for 2020.	49
Figure 4.7.4: As Figure 4.7.1 for 2021.	49
Figure 4.8.1: The relationship between CO ₂ flux and temperature and water concentration in 2018. Data were measured by YAJP tower.	50
Figure 4.8.2: As Figure 4.8.1 for 2019.	51
Figure 4.8.3: As Figure 4.8.1 for 2020.	51
Figure 4.8.4: As Figure 4.8.1 for 2021.	52
Figure 4.9: Photosynthetically Active Radiation (PAR) in 2018 to 2021. Data were measured by YAJP tower.	53
Figure 4.10: (a): Average CO ₂ concentrations with wind direction from August 2018 to July 2020. (b): Average CO ₂ fluxes with wind direction from August 2018 to July 2020. (c): Average SO ₂ concentrations with wind direction from June 10 to 17, 2018.	55
Figure 4.11: The wind direction coordinates at YAJP tower. The radius of circle is 20km. The red triangle is Syncrude stack location, and the yellow triangle is Suncor stack location.	57
Figure 5.1: Red line is the average of temperature and water vapour concentration of 15 days in March/April of each year from 2018 to 2021 at YAJP site, black line is annual	

average temperature and water vapour concentration values at JP104 site.....	59
Figure 5.2: CO ₂ concentration (red lines) compared with temperature (black line) and water vapour (blue line) of 15 days in March/April of each year from 2018 to 2021.....	60
Figure 5.3: CO ₂ flux (red lines) compared with temperature (black line) and water vapour (blue line) of 15 days in March/April of each year from 2018 to 2021.....	61
Figure 5.4: CO ₂ concentration (red lines) and CO ₂ flux (purple line) compared with PAR (yellow line) of 15 days in March/April of each year from 2018 to 2021.....	62
Figure 5.5: CO ₂ concentration (red lines) compared with CO ₂ flux (green line) of 15 days in March/April of each year from 2018 to 2021. (Added a legend to the image)	63
Figure 5.6: Comparison of monthly average CO ₂ concentration measured by YAJP tower and global monthly mean CO ₂ concentration measured by Global Monitoring Laboratory (GML).....	65
Figure 5.7: CO ₂ flux measured at the YAJP tower in Aug.25 th , 2021.....	67

List of Table

Table 1: The location, model and height of the instruments on the YAJP tower. Intensive measurements are those that were only completed in July 2017, June 2018, and August 2021. Continuous measurement refers to measurement that continues throughout the winter. A tick indicates that the instrument was used in the corresponding year..... 27

Table 2: Net ecosystem production (NEP) in different forest..... 68

1. Introduction

Forests are the main source of most of the carbon, water and energy flux between the land surface and the atmosphere (Margolis, 1997). 9% of the Earth's land is forest (Adams, 2012). In 2010, 34% of the land in North America was covered by forests, accounting for 17% of the global forest cover (FAO, 2010). The boreal forest is one of the largest biological communities on the Earth, consisting of alpine forests, wetlands and lakes, and is dominated by coniferous forests, with an area of about $14.7 \times 10^6 \text{ km}^2$ (Margolis, 1997). Therefore, northern forests play an important role in the global carbon cycle. It is estimated that the global forest carbon storage is $861 \pm 66 \text{ PgC}$, with an increase of $2.4 \pm 0.4 \text{ PgC yr}^{-1}$ (Pan et al., 2011). Increased human activities, such as the burning of fossil fuels, have led to an increase in greenhouse gases. Carbon dioxide is one of the main greenhouse gases. The increase in carbon dioxide will have an important impact on the carbon balance between forests and the atmosphere (Juurola, 2016).

There are about 309 Mha of forest in Canada, including other woodlands (Brandt et al. 2013). These woodlands account for about 27% of the global tundra forest and 8% of the global forest area (Brandt et al. 2013). Therefore, the carbon balance and carbon absorption of the boreal forests of Canada will affect the global atmospheric carbon budget and the stability of global carbon dioxide (Kurz et al., 2019). It is necessary to monitor the emission and absorption of carbon dioxide in the boreal forests of Canada.

For net carbon dioxide fluxes, the exchange between the forest and the atmosphere consists of leaf photosynthetic fluxes and fluxes of organisms in the soil (e.g., respiration by plant roots). (Ruimy et al., 1995). Solar radiation, air temperature, soil temperature and humidity, light duration, leaf area and seasonal changes are all important factors affecting carbon balance (Baldocchi, Vogel & Hall, 1997). The carbon dioxide flux also change in different seasons and different sunlight intensity. This project focuses on boreal forests because they are considered by climatologists as a potential carbon sink and are of great research value (Baldocchi, Vogel & Hall, 1997). Climatologists point out that if large amounts of

greenhouse gases are emitted, large-scale temperature disturbances may occur in boreal forests. Specifically, as the climate warms and the soil dries, it will weaken the carbon storage of the boreal forests, and the forests will begin to release carbon dioxide into the atmosphere (Kurz, Shaw & Boisvenue, 2019).

Therefore, understanding the carbon exchange process between the forest ecosystem and the atmosphere, understanding how human activities directly or indirectly affect the forest ecosystem and the atmosphere, and understanding the changes in atmospheric carbon dioxide can help better understand the impact of global warming on the forest.

The goal of this project is to study the exchange of CO₂ fluxes in the boreal forests near oil sands processing facilities in recent years and the factors affecting CO₂ exchange. The difference between this project and previous studies is that the trees in the study area of this project consist of jack pine trees, while the previous boreal forest studies are mainly black spruce forest or mixed forest. Also, the study area is near the oil sands facilities, which allows the investigation of nearby pollutants on CO₂ exchange in the forest.

The carbon balance of the boreal forest near the oil sands facility mainly depends on the difference in two main fluxes: absorption (net primary production) and decomposition release (anaerobic respiration). The carbon balance will be affected by many factors. This project study the influence of temperature, wind speed, water vapour concentration, and photosynthetically active radiation (PAR) on CO₂ concentration and flux. However, the factors affecting exchange of CO₂ concentration and CO₂ flux may not only include the above-mentioned aspects but may also include effects from pollutant plumes released by oil sands facilities. This project use short-term SO₂ measurements to determine under what conditions the pollution released by smokestacks will be carried to the forest near the boreal forest site. This can help to determine if the pollution affects CO₂ exchange.

1.1 Boreal Forest in Canada

The data (including forest carbon stocks, changes in carbon stocks, and greenhouse gas emissions) on the carbon balance estimates for managed forests in the Boreal Forest Region is from National Forest Carbon Monitoring, Accounting and Reporting System (NFCMARS), which is a national system for monitoring and reporting forest carbon (Kurz, 2013). As shown in Figure 1.1, NFCMARS monitors forests throughout Canada, including: boreal managed, boreal unmanaged, non-boreal managed, non-boreal unmanaged, continuous permafrost, and discontinuous permafrost. Of the 270 Mha of boreal forest area in Canada, 145 Mha of forests are identified as managed forests (which are defined as the careful management and adjustment of forests to meet human needs without harming the overall health of the forest (FAO, 2010)) for monitoring and reporting of greenhouse gas emissions and removals. 125 Mha of forest is not officially managed for the purpose of protecting the natural ecology and giving priority to the natural development of the forest, so it is called an unmanaged forest (Brandt, 2013). The boreal forest area is shown in Figure 1.1.

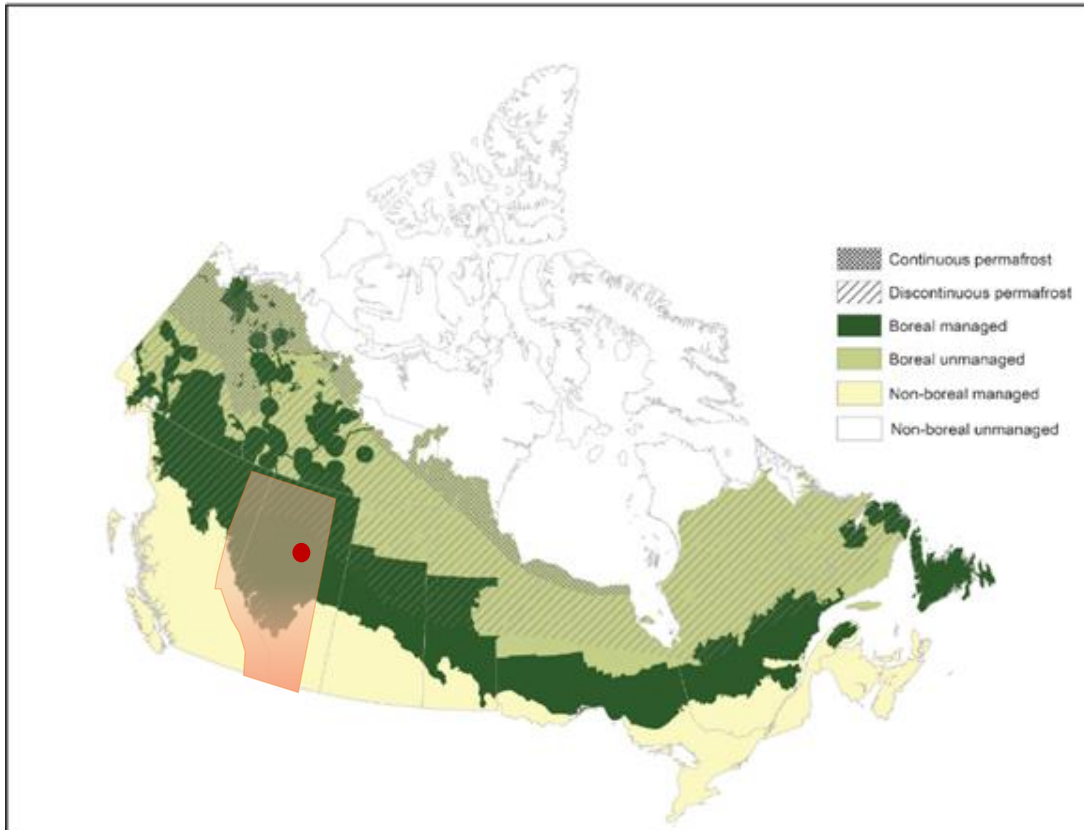


Figure 1.1: Kurz et al. (2013). Geographic relationship between the boreal zone as defined by Brandt (2009), the managed forest as defined by Canada for the purposes of reporting to the UNFCCC (Stinson et al. 2011), and permafrost zones (Hegginbottom et al. 1995). The orange area is Alberta where the study area is located. The red dot is the Athabasca oil sands region.

For managed boreal forest, Kurz et al. (2013) pointed out that the carbon balance of the boreal forest managed by Canada is mainly affected by the net balance of two fluxes, carbon uptake (net primary production) and decomposition release (heterotrophic respiration). They also proposed that in addition to the two major fluxes of managed boreal forests, carbon balance would also be subject to human or natural disturbances at specific times, such as excessive logging, fires and insect disasters that would interfere with the number and survival of trees.

The carbon balance of coniferous forests in unmanaged boreal forest regions is determined by natural processes that affect growth, death, and decomposition. Among them, fire

caused by lightning is the main natural disturbance, and other natural disasters, such as insect disasters, also have relatively small impacts (Hayes et al. 2012; Huntzinger et al. 2012). There is no commercial harvesting in unmanaged forests because the trees are low productivity and are limited by low temperatures, short growing seasons, permafrost, low decomposition rates and low nutrients (Graven et al. 2013). Theoretically, the inverse model can be used to estimate the carbon balance in unmanaged areas, but the calculated conclusions have no spatial resolution, for example, it is not possible to estimate the length of the growing season of trees, also it is not possible to estimate which areas are low decomposition rate areas or low nutrient areas, and some areas are permafrost areas, so it is hard to determine whether the net change in fluxes remains in balance (Graven et al. 2013).

2. Background

2.1 Related work

2.1.1 The exchange of carbon dioxide between vegetation and the atmosphere

The growth of trees depends on the water, nutrients and carbon dioxide in the air. Plants absorb carbon dioxide as energy for their own growth. In principle, the more trees there are, the less carbon dioxide there is in the atmosphere (Juurola, 2016). The annual carbon dioxide absorbed by the forest from the atmosphere accounts for about one-third of the annual emissions of fossil fuels (Juurola, 2016). The interaction between the forest ecosystem and the atmosphere is mainly related to carbon dioxide, water vapour and energy flux (Hari, 2012). So it is very important to study the changes of carbon dioxide in the forest.

In forests, the exchange of carbon dioxide between vegetation and the atmosphere is mainly accomplished by the absorption and release of carbon dioxide by vegetation. This process depends on the pores on the plant surface. Moreover, the leaves, trunks and stems of vegetation can exchange carbon dioxide. This process is affected by many factors, the most direct of which is solar radiation. Photosynthesis varies with the change of light intensity, but excessive sunlight increase the temperature and reduce the air humidity (Juurola, 2016). When the temperature is too high and the air humidity is too low, it will affect the amount of liquid water in the plants, which is called transpiration. When the transpiration is too high, it will cause the stomata of the plant to close, so as to avoid the death of the plant due to dehydration (Juurola, 2016).

Forests release energy through respiration, and then water and carbon dioxide become respiratory products released into the atmosphere. Respiration not only occurs in leaves, trunks, and stems, but also in the roots under the soil (Juurola, 2016). The respiration of the roots and the decomposition of microorganisms both cause the soil to produce carbon dioxide and emit it into the air. Respiration is affected by temperature, but when soil moisture is too low, respiration will slow down (Juurola, 2016).

Although in the forest ecosystem of the tree canopy, the role of ground vegetation is significantly less than that of trees, in non-enclosed canopy ecosystems, sunlight can illuminate low shrubs, mosses, herbs, turf and other ground vegetation through gaps. These plants also exchange gas with air and generate carbon cycles in the ecosystem and surrounding environment (Hari, 2012).

As shown in Figure 2.1, in a boreal forest at Hyytiälä Forestry Field Station located in Juupajoki, Southern-Finland (Juurola, 2016), during the year, spring provides good sunlight for plant growth, but because the air is dry and temperature fluctuates below zero, there is a risk of freezing. Usually, trees enter the state of metabolic activity at the end of spring. In summer, plant photosynthesis and respiration are most effective. The transpiration effect in summer is also very strong, the moisture in the soil decreases faster, and the trees accumulate energy in the next growing season. In autumn, the photosynthesis of the trees decreases, the trees stop growing, the leaves fall, and the plants harden in winter. The purpose of hardening is to reduce damage caused by icing. In winter, plants hibernate to protect themselves. And snow is a great waterlogger in winter, which will accumulate in the soil and provide moisture to the roots of the plants, as well as forming a protective layer to insulate them from cold air. (Juurola, 2016).

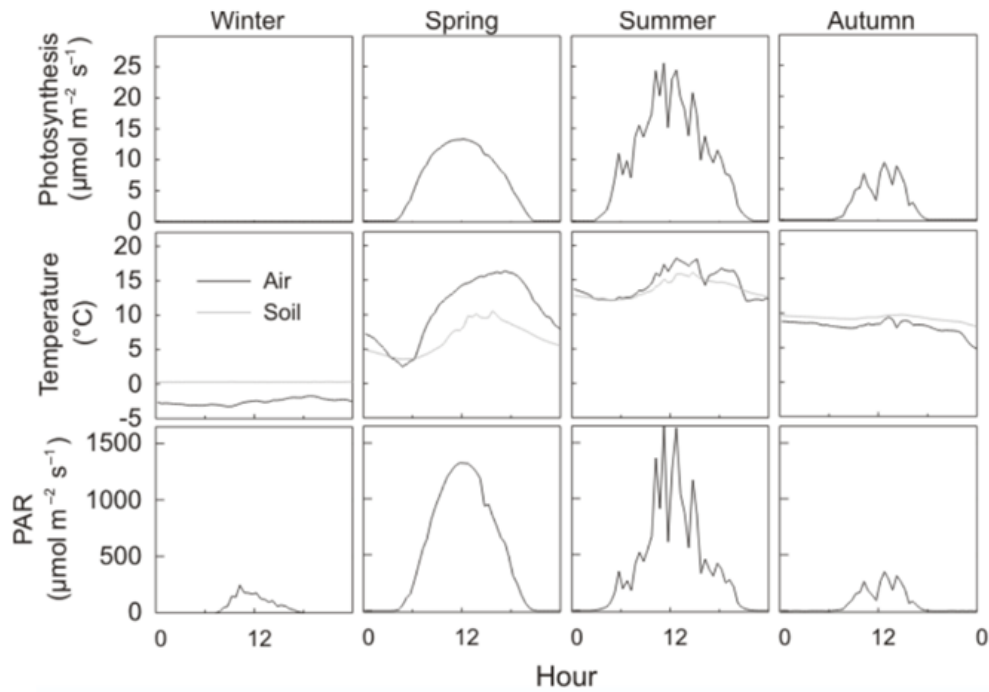
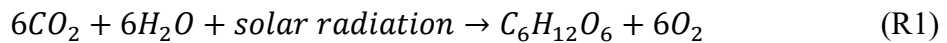


Figure 2.1: Juurola et al. (2016). Changes in light, temperature and photosynthesis of plants throughout the year at Hyytiälä Forestry Field Station located in Juupajoki, Southern-Finland.

2.1.2 CO₂ in the Boreal Forest

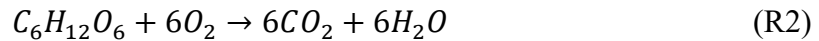
Greenhouse gases can absorb and emit radiation in the thermal infrared range, which will cause the greenhouse effect. CO₂ is the most important greenhouse gas. Due to human activities, such as the emission of fossil fuels, the concentration of CO₂ increased. Plants can absorb and release CO₂, thereby regulating the concentration of CO₂ in the atmosphere. The energy of plants comes from atmospheric carbon dioxide, water and sunlight. As shown in Figure 2.2, plants absorb CO₂ through photosynthesis and release CO₂ through respiration.

Photosynthesis is the process by which plants absorb CO₂, and plants exchange gas with the atmosphere through their stomata.



In order for plants to grow, they need energy. Respiration converts oxygen and sugar into

water and CO₂ to provide energy for plants.



Baldocchi et al. (1997) conducted experiments in the northern taiga located in Saskatchewan, Canada. Figure 2.3 compares the average day and night process and storage period of the net ecosystem carbon dioxide exchange (NEE). The figure shows that the storage of carbon dioxide was the largest from dawn to noon and after sunset. The carbon dioxide flux was negative in the morning. After photosynthesis begins, carbon storage in the air decreases and is minimal at noon. After sunset, photosynthesis stops, respiration starts, and carbon dioxide reserves became positive (Baldocchi et al. 1997). Figure 2.3 shows the changes in the flux of carbon dioxide during a day in the study area of this project as $NEE = F_C + F_{storage}$, where NEE is net ecosystem exchange, F_C is the carbon flux, and the $F_{storage}$ is carbon storage.

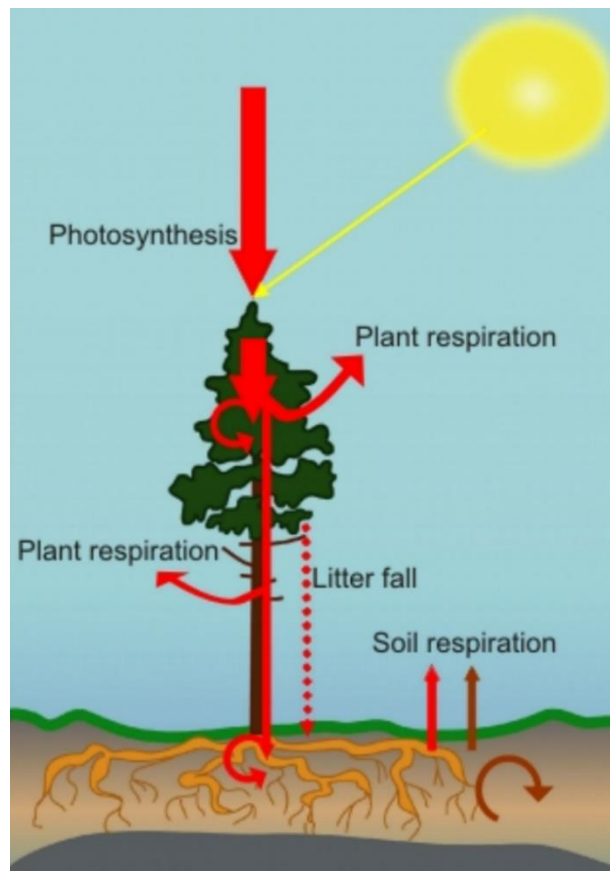


Figure 2.2: Eija Juurola et al. (2016). The capture and release of carbon dioxide (CO₂) by the forest.

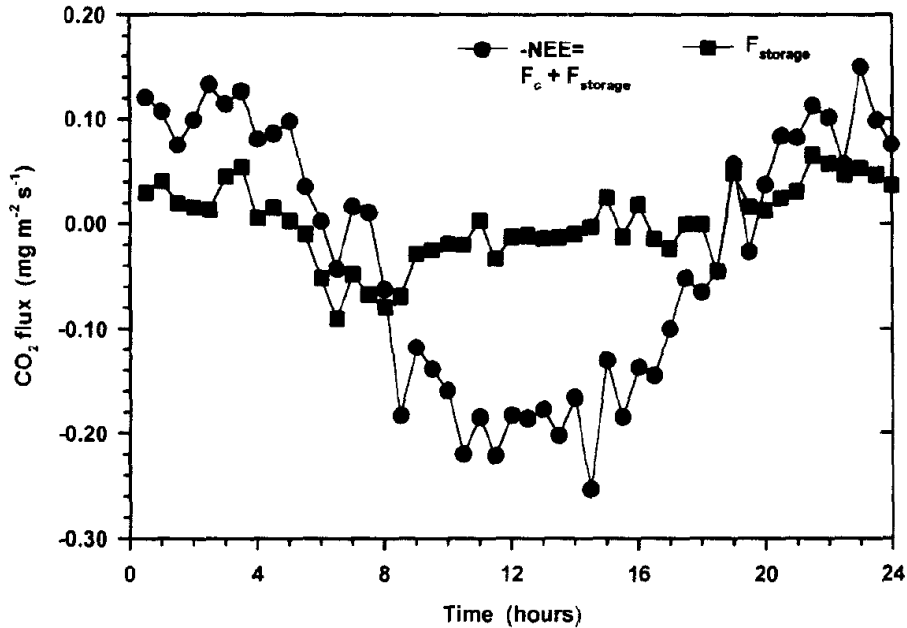


Figure 2.3: Baldocchi et al. (1997). A typical diurnal course of net ecosystem exchange (NEE) of CO₂, and the flux (F_c) associated with the storage (F_{storage}) of CO₂, in the underlying air layer.

2.1.3 Pollution released by oil sands region.

Oil sand ore is an important source of Canadian crude oil (CAPP, 2018). Canada's largest oil sands mines are located in Alberta, which includes Athabasca Peace River and Cold Lake deposits (CAPP, 2018). Oil sands are a mixture of sand, water and bitumen (CAPP, 2018). These oil deposits are located under the boreal forests and peat bogs of Alberta, with approximately 170 million barrels (CAPP, 2009). Approximately 20% of Alberta's oil sands are mined in open pits, which destroys the ecological health of boreal forests (Alberta Energy, 2018). Oil sands mining is one of the main sources of anthropogenic greenhouse gas emissions. The five major air pollutants produced by oil sands mining include: carbon monoxide (CO), nitrogen oxides (NO_x), sulfides (SO_x), ammonia (NH₃), particulate matter (PM) and volatile organic compounds (VOC).

Oil sands development requires energy, and burning natural gas provides energy for development, so the development of oil sands require about 1 billion cubic feet of natural gas every day. Burning natural gas release a large amount of carbon dioxide (David, 2008).

Due to the many processes involved in oil sands development, processing is more difficult, which causes the carbon dioxide emitted by oil sands production to be 5% to 15% higher than the carbon dioxide produced by crude oil development (Timothy, 2009).

The carbon dioxide released by oil sands processing facilities accounts for 12% of Canada's greenhouse gas emissions (CAPP, 2018). The release of CO₂ from smokestacks affects the CO₂ balance of forests. Winds from different directions bring pollutants into the forest, which may affect the absorption and release of carbon dioxide by plants.

2.1.4 Turbulent fluxes and spectra

Micrometeorological processes occur in the atmosphere and lower surfaces, including forests. These processes are generally accompanied by the exchange of energy and gas, which will produce fluctuations in a measured time series. When carbon dioxide is transported to or from the forest canopy, it is exchanged between the canopy and the atmosphere. By measuring this exchange, we can study the absorption of carbon dioxide in the forest (Foken, 2008).

Turbulence is the state of fluid flow. When the fluid flow velocity is large, there are many small vortices in the flow field, the laminar flow is destroyed, not only wind shear, but also the mixing between adjacent flow layers, forming turbulence (Foken, 2008). For the calculation of turbulent exchange, the eddy covariance calculation can be used. Eddy covariance is an atmospheric measurement technique that can be expressed mathematically as:

$$F = \overline{\rho_a w' s'} \quad (1)$$

where $\overline{\rho_a}$ is mean air density, w' is fluctuation of vertical wind speed from the mean value, and s' is fluctuation of a mixing ratio from the mean value.

In Figure 2.4, $E(k)$ represents the contribution to the total kinetic energy for wave numbers between k and $k + dk$. $E(k)$ reaches a peak in the energetic region and is zero at both ends of the spectrum. It is mainly composed of three spectral regions (A, B, C). The

area A is the area of energy production, which contains most of the turbulence energy and the energy generated by buoyancy and the shear force. Area B is an inertial sub-range area, in which energy is neither be generated nor consumed, but is transmitted to smaller and smaller scales. The C area is the dissipation area, in which kinetic energy is converted into internal energy. At the Eulerian integral length scale $k \sim 1/\Lambda$, $E(k)$ is the maximum value (Kaimal, 1994).

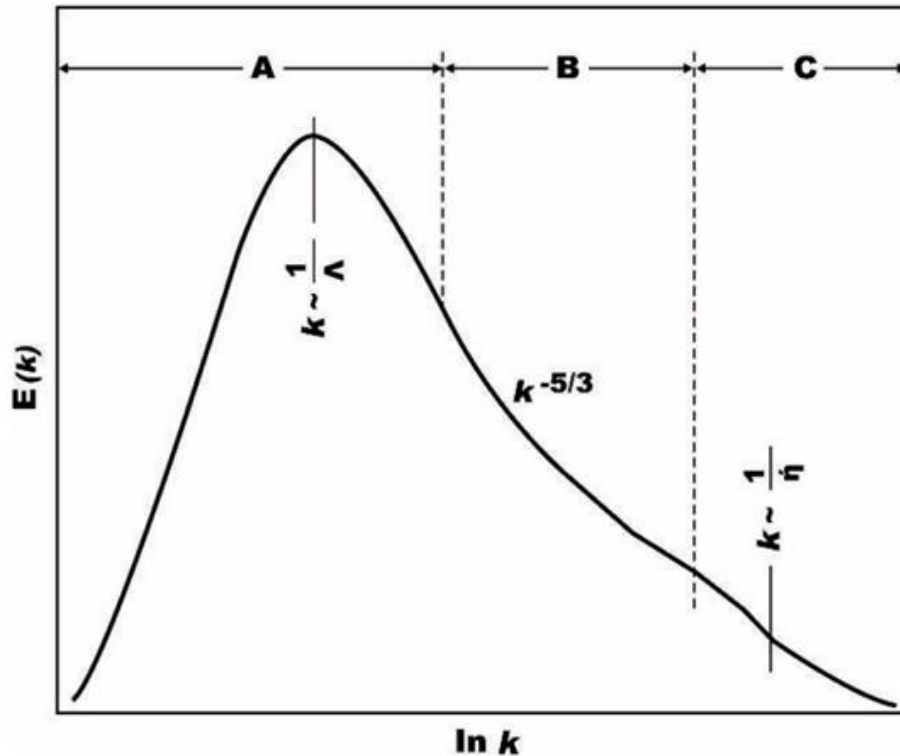


Figure 2.4: Foken et al. (2008). Schematic plot of the turbulence spectra and the ranges of energy production (A), the inertial sub-range (B) and the dissipation range (C) dependent on the wave number k (Kaimal and Finnigan 1994)

2.1.5 Research tasks

Boreal forests contain forests of many different tree species, such as black spruce, jack pines, and mixed forests. The YAJP site studied in this project is a pure jack pine forest, so it complements the type of boreal forest study. Because the boreal forests studied in the early years were mainly dominated by black spruce or mixed forests, such as Borden Forest.

This project investigated the effects of temperature, wind direction, humidity and light intensity on CO₂ concentration and flux. To determine the main factors affecting CO₂ exchange. The trends of temperature, H₂O concentration, and light intensity from 2017 to 2021 were analyzed, and their changing trends were found. The trends of CO₂ concentration and CO₂ flux are also summarized (see sections 4.4 to 4.8). However, the impact on CO₂ exchanges from oil sands processing facilities is also important. Therefore, the project also summarizes the short-term SO₂ data measured by YAJP and compares it with wind direction to determine under what conditions the pollution released by the smokestacks will be carried into the forest near the YAJP tower (see section 4.10). After determining the directions of pollutants, compared the differences in CO₂ concentration and CO₂ flux from these directions with other directions without pollutants. This could clarify whether oil sands development facilities affect forest carbon dioxide exchange.

2.2 CO₂ fluxes of different forests

The Borden Forest Research Station is located in Ontario, Canada at 44.318N, 79.934W, which is in the temperate to northern transition zone between 44° and 47° north latitude. The forest is a mixed and mature forest, which contains *Acer rubrum*, *Pinus strobus* and *Quercus rubra* (Latin name) in temperate forests in the south, as well as Black Spruce and Jack pine in the north. The height of the canopy is approximately 22 m, and the height of the infrastructure of the CO₂ measuring tower is 42 m. The environment in this area is susceptible to climate change, and small changes in climate may cause major changes in forests (Froelich et al., 2015).

Froelich et al. (2015) analyzed 17 years of data (Figure 2.5) from the Borden forest. They conclude that the forest is a low-to-medium sink with an average CO₂ budget of 177 g C/m²/yr.

Another boreal forest is located in the black spruce base 75 kilometers southeast of Chibougamau, Quebec, Canada (Giasson, 2006). The area is 400 meters above sea level,

with a lot of industrial and forestry activities, medium soil and good drainage (Giasson, 2006). Giasson et al. used the eddy current covariance technique to calculate the change in carbon dioxide exchange in the area, and the results showed that the carbon dioxide flux in the area increased from 111 g C/m²/yr to 175 g C/m²/yr due to human disturbance.

Bergeron et al. (2007) studied the Eastern Old Black Spruce (EOBS) sites located at the junction of the southern and northern boreal forests in 30 kilometers south of Chibougamau, Quebec. It is mainly covered by black spruce, with a few conifers and larch (Bergeron, 2007). Bergeron et al. found that the EOBS site is a neutral carbon sink with an annual total NEP (net ecosystem production, which is the difference between the gross primary product and the total respiration of the ecosystem) of 4±8 g C/m²/yr. They also studied Southern Old Black Spruce (SOBS), located 100 kilometers northeast of Saskatchewan. The terrain is flat, dominated by black spruce, with a small amount of larch and jack pine. The SOBS site is a weak carbon sink with a total annual NEP of 30±5 g C/m²/yr (Bergeron, 2007).

The Northern Old Black Spruce (NOBS), located 40 kilometers west of Thompson, Manitoba, is located on the edge of the boreal forest in the northern part of the discontinuous permafrost. It is a mixture of highland forests and swamps (Bergeron, 2007). The area is well-drained and dominated by dense 10-meter-high black spruce, with an annual total NEP of 27±11 g C/m²/yr (Bergeron, 2007).

The Hyytiälä Forest Site is closer to the Arctic Circle. The Hyytiälä Forest Farm Monitoring Station is located in Juupajoki (Juurola, 2016) in southern Finland. The forest type in this area is lingonberry type, with pine trees as the main height of about 17m, which is slightly different from the canopy height studied in this project. The soil at this site is formed by glacier water formed by the melting of glaciers 115,000 to 10,000 years ago, and various rocks and soil particles are left where the glaciers melted (Hari, 2012). Mammarella et al. (2007) used long-term eddy current covariance to measure CO₂ flux at the SMEAR II field station (Hyytiälä, Southern Finland). As shown in Figure 2.6, the annual CO₂ flux in Hyytiälä Forest is 4.74 μmol/m²/s (Mammarella 2007).

Chi et al. (2021) studied two mature spruce-pine mixed forests near northern Sweden, a pine forest and a spruce-pine forest. They used the cospectra model to measure the net forest floor CO₂ exchange (NFFE) of the forest and the entire net ecosystem CO₂ exchange (NEE). However, the spruce-pine mixed forest had higher ground respiration and lower photosynthesis, which was 1.4 times the net CO₂ source of the pine forest (Chi, 2021). The gross primary product (GPP) of the two forests was similar, so the main reason for this difference was the net forest floor CO₂ exchange (NFFE) (Chi, 2021). Therefore, the CO₂ flux on the forest floor plays an important role in regulating the carbon balance of the boreal forest, and it has a greater impact on the flux than the upper part of the forest canopy (Chi, 2021).

Gross Ecosystem Production (GEP) is the chemical energy created by primary producers in a given period of time, usually expressed as carbon biomass. Ecosystem respiration (RE) refers to the sum of all the respirations of organisms in the ecosystem. These two processes constitute the basic function of the overall respiration of the ecosystem. The expression of the relationship between NEP, RE and GEP is:

$$NEP = GEP - RE \quad (2)$$

The terminology generally refers to the use of carbon dioxide and water in photosynthesis, the production of glucose and oxygen in the sun, and the use of glucose and oxygen to produce carbon dioxide and water in cell respiration and energy (Yvon-Durocher, 2012).

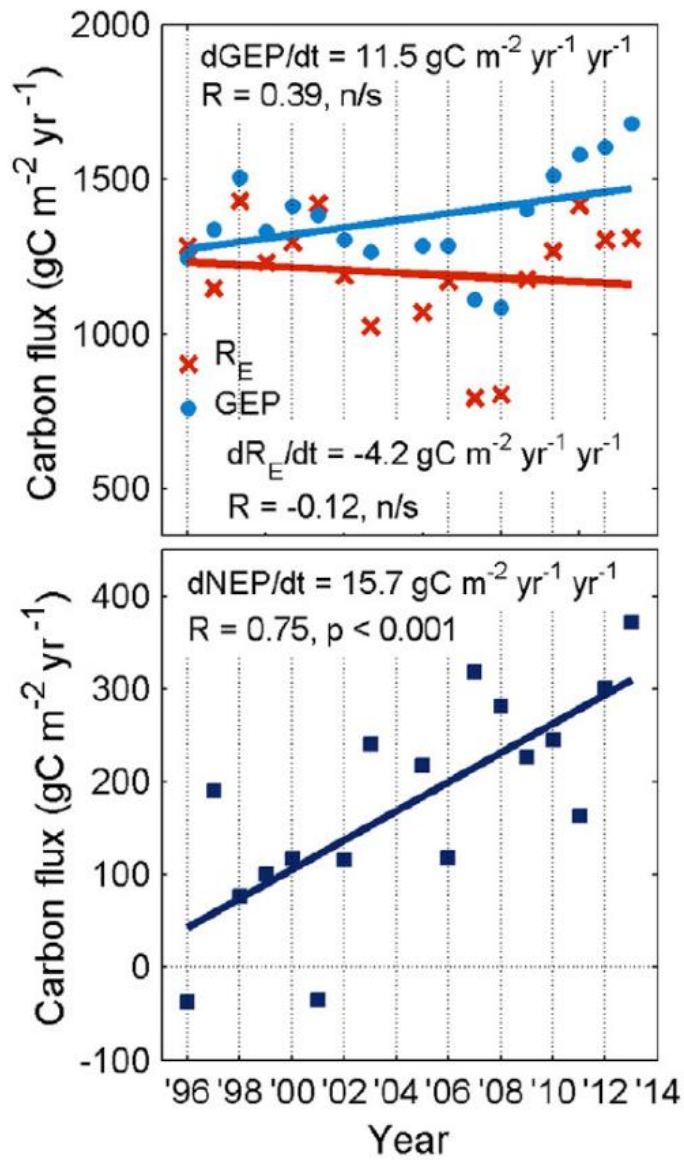


Figure 2.5: Froelich et al. (2015). Annual totals of gross ecosystem productivity (GEP), ecosystem respiration (RE), and net ecosystem productivity (NEP).

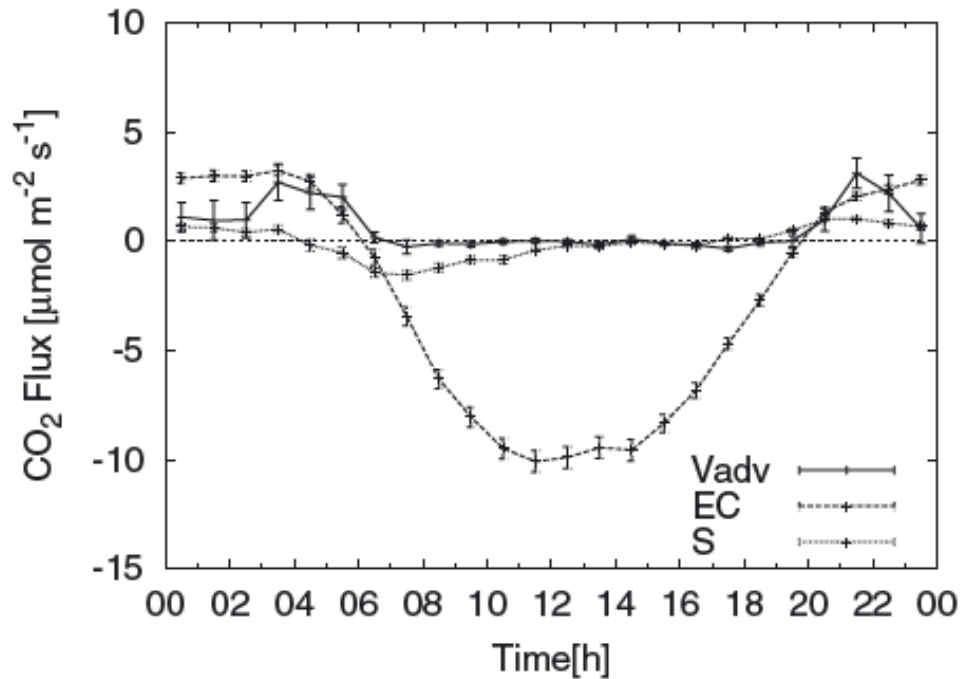


Figure 2.6: Mammarella et al. (2007). Mean diurnal course of CO₂ fluxes with standard error bars for the summer 2004 in Hyytiälä Forest.

2.3 The impact of different vegetation on CO₂ changes (forest, moss, lichen)

In British Columbia, Canada, the photosynthesis of forest stratum is dominated by moss and lichen and is limited only by light, temperature and moisture (Botting and Fredeen, 2006). The instantaneous forest floor net ecosystem CO₂ exchange (ffNEE) values of moss measured by Botting and Fredeen in the Aleza Lake Research Forest (ALRF) forest which is approximately 60 km northeast of Prince George, in central British Columbia, Canada, range from -2.7 to +3.6 μmol/m²/s, and the instantaneous ffNEE values of lichen range from -2.0 to +4.4 μmol/m²/s. They also pointed out that the moss in this woodland increase the photosynthesis by increasing the CO₂ concentration. For example, at a CO₂ level of 700 ppm, the average measured total photosynthesis of the moss is 1.19 μmol/m²/s. At 430 μmol/mol, the average measured total photosynthesis of the moss is 1.08 μmol/m²/s. On the contrary, the photosynthesis of lichen decrease with the decrease of CO₂ concentration. There are many conditions that affect the photosynthesis of trees. In addition to light,

temperature and moisture, there are also conditions such as soil moisture, soil temperature, and plant stomata. Moreover, trees are much higher than ground plants, so the CO₂ flux at high places is easily affected by the weather and forms of turbulence.

Compared to trees, moss and lichens absorb less CO₂ and are less affected by these factors.

2.4 Changes in the CO₂ flux of the forest after fire

Köster et al. (2018) studied the changes in CO₂ flux in the boreal forests of Siberia after a fire, and as shown in Figure 2.7, they found that the time of the fire and CO₂ emissions are positively correlated ($R = 0.408, p = 0.0010$). The soil carbon storage of the burned area a year ago was 74% smaller than the oldest burned area, and the carbon dioxide emissions dropped by about 75%. Their research results show that in the recently burned areas, the vegetation and root systems have died on a large scale, resulting in a reduction in CO₂ emissions in the absence of vegetation. However, most of the vegetation and root systems in areas that burned 56 years ago or earlier have returned to normal, so CO₂ emissions will increase, and vegetation previously destroyed by the fire will be brought into the soil and become part of the carbon sink.

The fire have a very large impact on the forest, especially the composition and structure of the forest. After the fire, the vegetation have to undergo a long succession and activities to recover, and the recovery time of the permafrost areas is much slower (Köster, 2018).

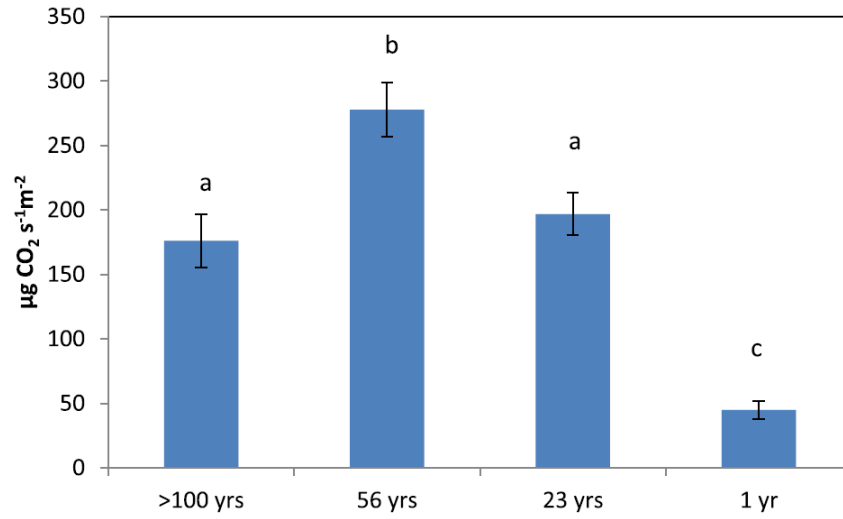


Figure 2.7: Köster et al. (2018). Average carbon dioxide (CO₂) flux (µg CO₂ m⁻²s⁻¹) (n=72 per measurement period) per analyzed fire age class. Vertical bars represent the standard errors.

2.5 Modeling of CO₂ fluxes

The Community Land Model (CLM5.0, https://escomp.github.io/ctsm-docs/versions/release-clm5.0/html/tech_note/index.html) is a series of global land models developed by the Land Model Working Group (LWMG) of the Community Earth System Model (CESM) and maintained by the National Center for Atmospheric Research (NCAR). CLM5.0 uses the Medlyn stomatal conductance model to calculate stomatal conductance (Medlyn et al., 2011). The Medlyn model calculates stomatal conductance (the inverse of resistance) based on net leaf photosynthesis, vapour pressure deficit, and CO₂ concentration on the leaf surface (Medlyn et al., 2011). Leaf stomatal resistance is:

$$g_s = \frac{1}{r_s} = g_0 + 1.6 \left(1 + \frac{g_1}{\sqrt{D}}\right) \frac{A_n}{c_s/P_{atm}} \quad (3)$$

where r_s is leaf stomatal resistance (s m²/µmol), g_0 is the minimum stomatal conductance (µmol/m²/s), A_n is leaf net photosynthesis (µmol CO₂/m²/s), c_s is the CO₂ partial pressure at the leaf surface (Pa), P_{atm} is the atmospheric pressure (Pa), and D is the vapour pressure deficit at the leaf surface (kPa). g_1 is a plant functional type dependent parameter. Stomatal conductance (g_s) is an index to measure the degree of

stomatal opening, and this index can be used to describe the water status of plants. The reduction of stomatal conductance can prevent excessive loss of plant water by reducing transpiration. Botanists classify plants by their physical, phylogenetic and phenological characteristics, which are related parameters of plant functional types (g_1). This parameter is an important part of studying climate models. The accuracy of the CLM5.0 model is a root mean square error of no more than $0.04 \text{ cm}^3/\text{cm}^3$ (Gao, 2021).

The leaf net photosynthesis response curve is:

$$A_n = \frac{A_{max} + \alpha I - \sqrt{(A_{max} + \alpha I)^2 - 4\eta\alpha I A_{max}}}{2\eta} \quad (4)$$

where A_{max} is the high-light asymptote of that equation ($\text{kg CO}_2/\text{m}^2/\text{s}$), I is the Photosynthetically active radiation (PAR) ($\text{mol}/\text{m}^2/\text{s}$), η determines curvature of the hyperbola, and α determines the slope of the curve. This is based on a nonrectangular hyperbola describing photosynthesis in a mature C_3 leaf (Thornley, 1998). The equation is the response of leaf photosynthesis to light intensity and it varies seasonally within the canopy (Marshall, 1980).

CO_2 flux can be calculated using the following formula:

$$F = \frac{m_{CO_2} L C_{CO_2}}{r_s} \quad (5)$$

where m_{CO_2} is the molar mass of CO_2 , L is the total LAI of the forest (about 2 for our site), and $C_{CO_2} = c_s/P_{atm}$ is the mixing ratio of CO_2 .

3. Method

3.1 Study Site description

The York Athabasca Jack Pine (YAJP) Forest site area selected for the study is far from residential areas. The nearest town to the area is Fort Mackay, which is about 16 km northwest of the study site and has a population of approximately 700. The Ft. McMurray area is located 44 km south of the study site and has a population of approximately 66,000. The nearest highway is 650 m south of the study site, with sparse traffic and fewer vehicles compared to residential areas. Because there are fewer highway vehicles next to the study site and the study site is far from the town, the influence of the roadway and town on the measurements is considered negligible.

The York Athabasca Jack Pine Forest Site is characterized by its flat terrain and is composed of homogeneous jack pine trees. There are only a few sparse blueberry bushes in this area, and the ground is covered with reindeer moss. The average height of the forest canopy is between 19 and 22 meters, and as shown in Figure 3.1 the leaves of the trees are relatively sparse during the growing season. The leaf area index (LAI) of the forest near the YAJP site is estimated as $2 \text{ m}^2/\text{m}^2$ (Gordon, 2013). The site has a sandy ground with good drainage and is covered by snow in winter.

Although the study site is far away from the town, there are oil sands petroleum processing facilities nearby. The pollution detected in the research of this project mainly comes from the plume of oil processing facilities. Figure 3.2a illustrates the geographical location of the study area. As shown in Figure 3.2b, petroleum processing facilities around the study area include: Suncor facility about 13.5 km to the south-southwest of the study site; Syncrude facility located about 16 km to the southwest of the study site; the Shell Albian facility, which is approximately 13.5 km to the north of the study site; and the CNRL facility located approximately 31.2 km to the northwest of the study site. There is also an active rock quarry approximately 10 km to the northwest of the site.



Figure 3.1: From Jiang (2018). Boreal forest crown in the vicinity of the YAJP tower. Photo taken July 2017.

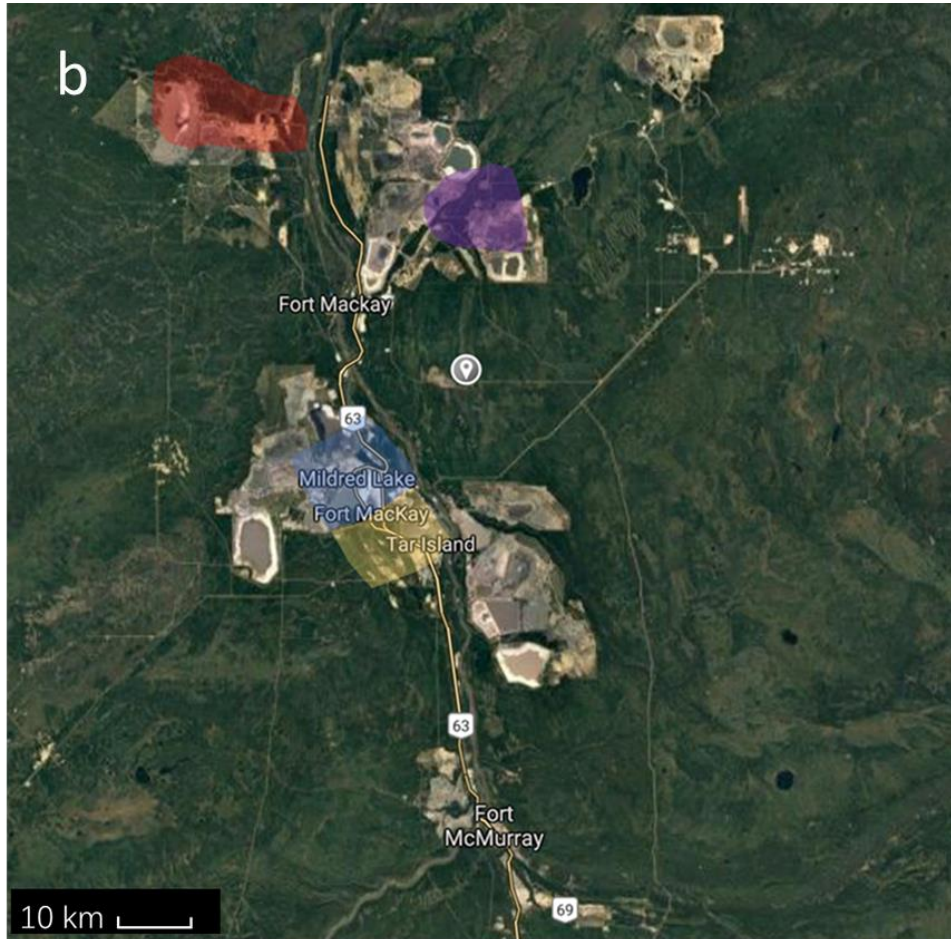


Figure 3.2: (a) The orange area is the location of the study area. (b) The grey spot indicates the YAJP tower site. The blue polygonal area is the Syncrude processing facility, the yellow polygonal area is the Suncor processing facility, the purple polygonal area is the Shell Albian processing facility, and the red polygonal area is the CNRL processing facility.

3.2 Study Site selection

The study site was selected in order to sample both clean air and polluted air. Polluted air is defined as wind from polluted regions, while clean air is defined as wind from region without oil processing facilities. Therefore, the selected location needs to have a period of clean air and polluted air, and there must be sufficient sampling. In order to find forest areas that meet the above characteristics, Jiang (2018) developed a stochastic back-trajectory model based on measurements from the Wood Buffalo Environmental Association (WBEA), which is a network of monitoring stations that provides hourly wind data. The model was used to calculate the probability of polluted air in each oil facility area. According to the results of Jiang (2018), the JP104 station (Figure 3.3. Wood Buffalo Environmental Association, 2019) of the WBEA monitoring network in summer measured 70% to 80% of the air to be from directions which would likely bring polluted air to the tower. Because JP104 (currently called Site 1004) is located in a forest area where clean air and polluted air can be collected (Jiang, 2019), and road access is possible, the YAJP tower was set 680 m north of JP104 station.

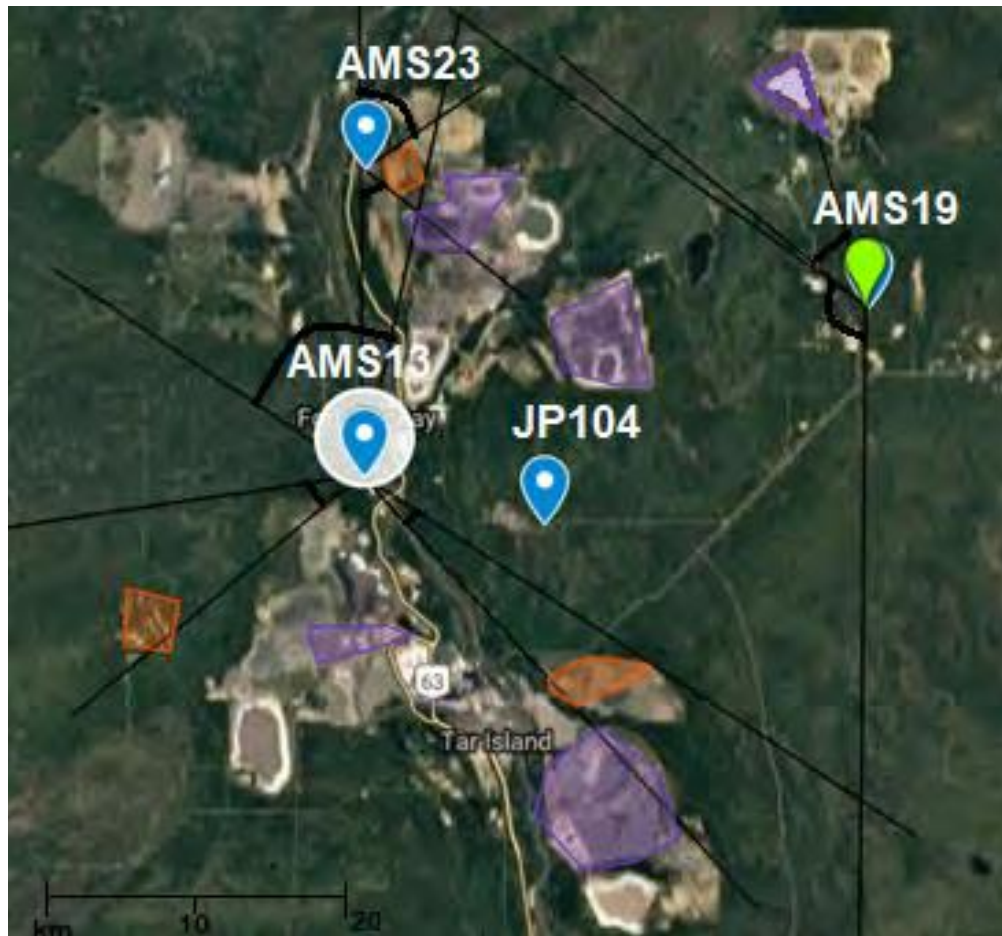


Figure 3.3: From Jiang (2018). Emission sources in the oil sands area. Purple polygons indicate emission sources. Orange polygons indicate possible sources which emit low amounts of particulates. These were determined by the emissions inventory in (ECCC 2016) and analysis from the WBEA data. Blue pointers indicate WBEA towers used in the Jiang (2018) analysis. Blue pointer with a white circle around it is AMS 13. Black lines delimit angles with elevated particulate concentrations; such angles lay in the sector with an arc.

3.3 YAJP tower and Instrumentation

The data of this research project are all measured from the YAJP tower. The YAJP tower was first installed in a small open space in the forest in July 2017. In the summers of 2017 (July), 2018 (June), and 2021 (August) intensive data collection and research were conducted. The tower was decommissioned in October 2021. SO₂ data was collected from the 9th to the 18th of June 2018. The tower is 31.4 m high and the surrounding tree canopy is between 19 m to 22 m in height (Figure 3.4). As shown in Table 1, from 2017 to 2021, different instruments were installed on the tower at different time periods. Table 1 shows the instruments installed on the tower, including: Sonic anemometers (ATI) installed at 31.4 m, 9 m, and 5.3 m; three Li-190 lights sensors (Li-Cor) were located at 31.4 m, 15.9 m and 1.3 m, and a CUV5 UV light sensor was located next to the 1.3m Li-190 light sensor; a Li-7500A CO₂/H₂O gas analyzer (Li-Cor) was installed at a height of 31.4 m and an LI-7500RS was installed at a height of 5.3 m; two DustTrak particle counters were installed at 16.6 m and 1.85 m; and three 2B ozone monitors were installed at varying heights. In the 2018 intensive study, a 43i SO₂ analyzer and a 49i Ozone analyzer (Thermo Scientific) were located next to an ultra-high sensitivity aerosol spectrometer (UHSAS, Droplet Technology Inc.) on the ground, but sampled from either 31.4 m or 2 m heights.

During the intensive collection of data in the field from 2017, 2018, and 2021, all instruments were powered by a generator, which was placed about 100 m northeast of the YAJP tower. Outside of the intensive field studies, all the remaining instruments were powered by batteries and recharged by solar energy. All the data measured by the equipment on the YAJP tower were remotely transmitted to a computer at York University through a cellular modem.

Table 1: The location, model and height of the instruments on the YAJP tower. Intensive measurements are those that were only completed in July 2017, June 2018, and August 2021. Continuous measurement refers to measurement that continues throughout the winter. A tick indicates that the instrument was used in the corresponding year.

Instrument	Sample Height [m]	Model and Remarks	Continuous (C) or Intensive (I)	2017	2018	2019	2020	2021
Sonic anemometer	31.4	Type A, ATI	C	√	√	√	√	√
Sonic anemometer	9	Type Vx, ATI	I	√				
Sonic anemometer	5.3	Type V, ATI	C	√	√		√	
Aerosol spectrometer	31.4	UHSAS, DTI.	I	√	√			√
Light sensor	31.4	LI-190, Li-Cor	C	√	√	√	√	√
Light sensor	9	LI-190, Li-Cor	C	√	√	√	√	√
Light sensor	1.3	LI-190, Li-Cor	C	√	√	√	√	√
UV sensor	1.5	Kipp-Zonen CUV5	C	√	√	√	√	√
Gas analyzer	31.4	Li-Cor LI-7500RS	C	√	√	√	√	√
Gas analyzer	5.3	Li-Cor LI-7500A	C	√				
O ₃ analyzer	2	Thermo Sci.	I		√			
SO ₂ analyzer	2 or 31.4	Thermo Sci.	I		√			√
Particle counter	16.6	DRX DustTrak	I	√				√
Particle counter	1.85	DRX DustTrak	I	√				√
Ozone monitor	5.6	2B 205	I		√	√		
Ozone monitor	0.9	2B 205	I	√	√	√		
Ozone monitor	Variable	2B 205	I	√				

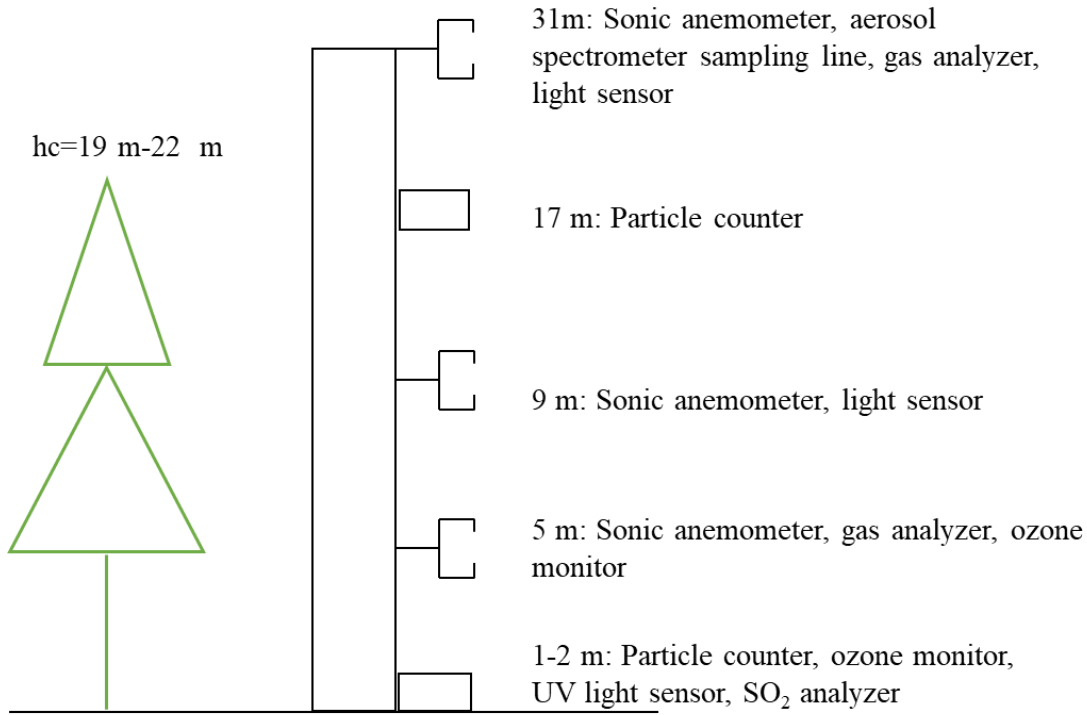


Figure 3.4: Schematic sketch of instrumentation placement on tower. Not to scale.

3.3.1 Sonic anemometers

In the project, the wind at the YAJP site is used for comparison with the concentration of CO₂ and SO₂. The sonic anemometer measures high-frequency wind speed. It works by emitting sound waves in the three coordinate axis directions. The wind speed of each component depends on the travel time of the sound wave between each pair of transducers.

The wind speed can be calculated by the following formula:

$$V_l = \frac{d}{2} \left[\frac{1}{t_1} - \frac{1}{t_2} \right] \quad (6)$$

where V_l is the component wind speed along the axis, d is the path length, and t_1 and t_2 are the time required for the sound wave to reach the other end from one end of the sensor.

The wind direction angle (θ) can be determined from the u and v components of the wind speed as:

$$\theta = 180^\circ + (180^\circ/\pi) * \tan^{-1} \left(\frac{u}{v} \right) - 11^\circ \quad (7)$$

where -11° refers to the angle of the sonic anemometer relative to true north.

The sonic anemometer used in this project can work and sample at high frequency (200Hz), but the frequency of this project is set at 10Hz (Jiang, 2019), which helps to transfer and process data.

3.3.2 Light sensors

Sunlight also affects the exchange of CO_2 . The LI-190 light sensor (LI-COR, Inc.) is used to measure photosynthetically active radiation (PAR) from wavelengths between 400 nm and 700 nm, which is the visible light that affects the photosynthesis of most plants. The response time of the LI-190 is less than 1 μs , and its sensitivity is $0.005 \mu\text{A s m}^2/\mu\text{mol}$.

The ultraviolet radiation meter CUV5 used in this project was designed by KIPP & Zonen. The wavelength range of ultraviolet radiation measured by CUV5 is 280nm to 400nm, its response time is 1 second, and the ultraviolet intensity can be measured up to 400 W/m^2 .

3.3.3 $\text{CO}_2/\text{H}_2\text{O}$ gas analyzers

The LI-7500 is a gas analyzer (LI-COR, Inc.) for measuring CO_2 and H_2O . It measured the mixing ratio of CO_2 and H_2O vapour at a height of 31 m. A second analyzer was mounted at a height of 5 m, which was functional for only part of the first year. It emits laser light at two frequencies and measures the attenuation of the laser light relative to the reference beam. The rate of attenuation is related to the gas concentration in its path.

The instrument measures millimole CO_2 per cubic meter, also measures temperature (T) and pressure (Pa). To convert to a mixing ratio of CO_2 , we assume standard temperature and pressure as $1 \text{ mg/m}^3=0.556 \text{ ppm}$ (since $44.01 \text{ mg/m}^3=1 \text{ mmol/m}^3$, so $1 \text{ mmol/m}^3=24.47 \text{ ppm}$).

Under normal operating conditions, the LI-7500 needs 30W to start up, and only 10W is needed for normal monitoring. For the continuous measurements, the YAJP tower instruments are powered by a solar panel and battery system. Therefore, the low-power LI-

7500 can complete long-term continuous measurement under solar power.

3.3.4 Thermo Scientific model 43i

The YAJP site is near oil sands development, so the surrounding forests are affected by pollutants released from oil sands processing facilities. Sulfur dioxide measured in this project is one of the pollutants. During the intensive studies of 2018 the mixing ratio of SO₂ was measured by the UV pulse fluorescence spectroscopy technique of a Thermo Scientific™ 43i model instrument. The analyzer can measure SO₂ up to 100 ppm in the air (Beecken, Mellqvist & Salo, 2014). The instrument uses an ultraviolet arterial light source to increase the light intensity, thereby generating greater ultraviolet light. The instrument has high sensitivity and a response time of 80 seconds. The Thermo Scientific™ 43i instrument is stable because it has a reflective bandpass filter, which is not prone to photochemical degradation and is more selective in terms of wavelength (Beecken, 2014).

3.4 CO₂ Eddy Covariance Measurement

The data for the CO₂ flux in the project came from the LI-7500 gas analyzer on the tower. The eddy covariance method is used to measure the CO₂ flux. The eddy covariance flux is calculated from Equation 1 as $F = \overline{w'n'}$, which represents the transmission of various quantities per unit time and unit area, where an overbar represents the average over a given time period, the prime represents the fluctuation from the mean, w represents the vertical wind, and n represents various quantities, such as gas or aerosol concentration (Foken, 2017). The eddy covariance measures net CO₂ exchange (i.e., NEE or NEP). When the measured conditions are nearly ideal, such as when atmospheric conditions (e.g., wind, temperature, humidity, CO₂) are very stable, the downcast vegetation is uniform and located on flat terrain with long upwind distances, the error of the net annual exchange of CO₂ is estimated as less than $\pm 50 \text{ g C / m}^2/\text{yr}$ (Baldocchi, 2003). In this project, $w\text{CO}_2$ refers to CO₂ flux and C refers to CO₂ concentration.

From the mass conservation equation:

$$\frac{\partial C}{\partial t} + \frac{\partial(u_i C)}{\partial x_i} = D_M \frac{\partial^2 C}{\partial x_i^2} + S \quad (8)$$

where C is the concentration, D_M is the Brownian particle diffusion coefficient, S is the source or sink, i is a summation index such that variables $(x_1, x_2, x_3) = (x, y, z)$ and wind speed $(u_1, u_2, u_3) = (u, v, w)$. Assuming that the concentration is horizontally homogeneous and stable, taking the Reynold's average value and integrating it over z , gives:

$$\int_0^{z_r} \frac{\partial \bar{C}}{\partial t} dz + \overline{w' C'}(z_r) = \int_0^{z_r} \bar{S} dz \quad (9)$$

where the first term is the storage flux F_s , the second term $\overline{w' C'}$ is the diffusion flux, and the third term is the source or sink. If the average is taken across many day and night cycles, assuming that the concentration is constant with height, then:

$$\bar{F}_s = z_r \frac{C(t+\Delta t) - C(t)}{\Delta t} = 0 \quad (10)$$

For our flux calculations we use 30 minutes as an average time period to analyze data and aggregate them to obtain a net flux.

Typically, the instrument measures the upwind region of the vertical turbulent flux, and the heat, water, and gas transport generated in this region is recorded by the instrument and is referred to as the flux footprint (Burba, 2008). The size of the flux footprint area is generally described using the term "fetch", which is the distance from the tower (Burba, 2008). The size of the flux footprint depends on the height of the tower, atmospheric stability, and surface roughness (Kljun, 2004). Since the study area is surrounded by at least 10 km of forest on all sides, we assume that the flux footprint contribution of the measured CO₂ fluxes comes from within this uniform region.

3.4.1 Removal of outliers

In practice, rain and snow, processing errors, and electronic noise, can cause outliers in the collected data. The so-called outlier data is erroneous data that is significantly higher in magnitude than the normal value.

For the gas analyzer, when it rains or snows, when the hydrometeor falls through the measuring path, it will affect the gas concentration measurement of the gas analyzer, causing the measurement to produce abnormal values, as shown in Figure 3.5.

For the sonic anemometer, when the hydrometeor falls through the sensor or measurement path, it will affect the transducer's ability to capture the correct signal.

In order to process and obtain valuable data, the data is generally processed every 30 minutes. Data outside of 3 standard deviations from the mean are removed as outliers. Three standard deviations were used because the data for CO₂ flux and CO₂ concentration were normally distributed, and outliers were defined as values in a set of measurements that deviate from the mean by more than three standard deviations. The process is then repeated on the new series until there are no outliers, as shown in Figure 3.6.

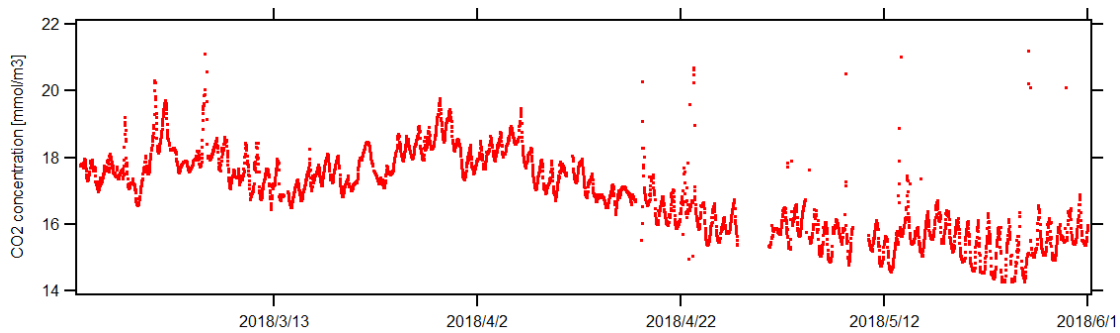


Figure 3.5: An example of raw CO₂ concentration data, with outliers.

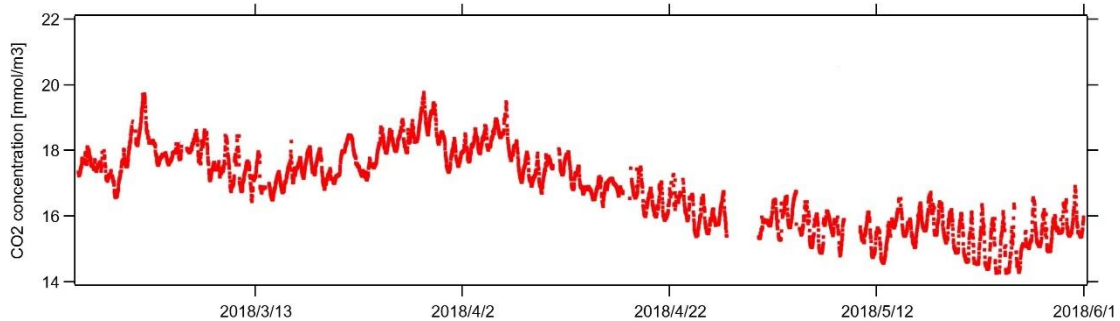


Figure 3.6: A sample of clean data (outliers removed).

3.4.2 Coordinate rotation

The basic condition for applying the eddy covariance method is to assume that the average vertical wind component is negligible, otherwise the advective flux must be corrected

(Wilczak, 2008). These rotations are used to correct the error in the vertical direction of the anemometer. This correction is called tilt correction and involves rotating the horizontal axis to the average wind direction. According to the rotation method proposed by Wilczak (2008): the first correction (Figure 3.7a) is to rotate the coordinate system around the z-axis to the average horizontal wind, where the angle of rotation is $\theta = \tan^{-1}\left(\frac{\overline{v_m}}{\overline{u_m}}\right)$:

$$u_1 = u_m \cos \theta + v_m \sin \theta \quad (11)$$

$$v_1 = -u_m \sin \theta + v_m \cos \theta \quad (12)$$

$$w_1 = w_m \quad (13)$$

where the u_m, v_m, w_m are the mean wind.

In the second step (Figure 3.7b), the coordinate system is rotated around the new y-axis until the average vertical wind is zero, where the second rotation angle is $\phi = \tan^{-1}\left(\frac{\overline{w_1}}{\overline{u_1}}\right)$:

$$u_2 = u_1 \cos \phi + w_1 \sin \phi \quad (14)$$

$$v_2 = v_1 \quad (15)$$

$$w_2 = -u_1 \sin \phi = w_1 \cos \phi \quad (16)$$

The second correction aligns the flow with the topography.

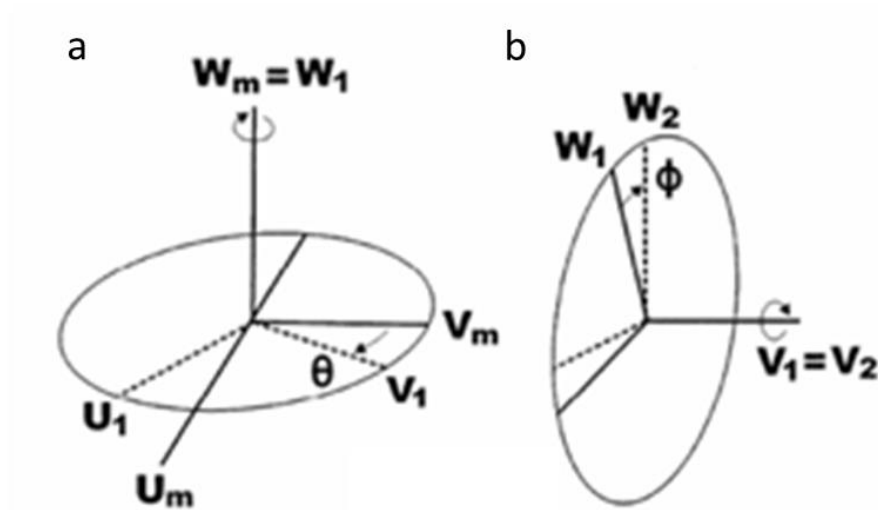


Figure 3.7: Wilczak et al. (2008). Definition of the coordinate rotations: (a) first rotation; (b) second rotation.

3.5 Data measurement

In this project, we measured data from August 2017 to August 2021. The measured data includes CO₂ concentration, CO₂ flux, H₂O concentration, H₂O flux, temperature, pressure, wind direction and wind speed. Figure 3.8 and 3.9 show examples of the 30-min averaged CO₂ concentration and CO₂ flux in all the data from August 2017 to August 2021. SO₂ data was measured only 9 days, from June 10th to 18th, 2018 (Figure 3.10).

Due to lack of power, all instruments stopped working in August 2018 (data collection stopped), but resumed work in November. From November 2018 to March 2019, due to the lack of sunlight in the winter forest, the batteries charged by solar panels can only provide electricity for the YAJP tower, and instruments installed on the tower were in a state of energy saving that stopped working, and then instruments resumed power in March 2019 to continue collecting data. The same situation also appeared from September 2019 to March 2020 and from December 2020 to February 2021. The lack of sunlight in winter also led to the lack of data. Therefore, the data collected between 2017 and 2021 were not continuous. The SO₂ data was collected during intensive field collection in June 2018. But the tower instruments weren't working for part of the 2018 study (because of a data-logger failure), so the hourly averaged wind direction data had to be obtained from nearby JP104.

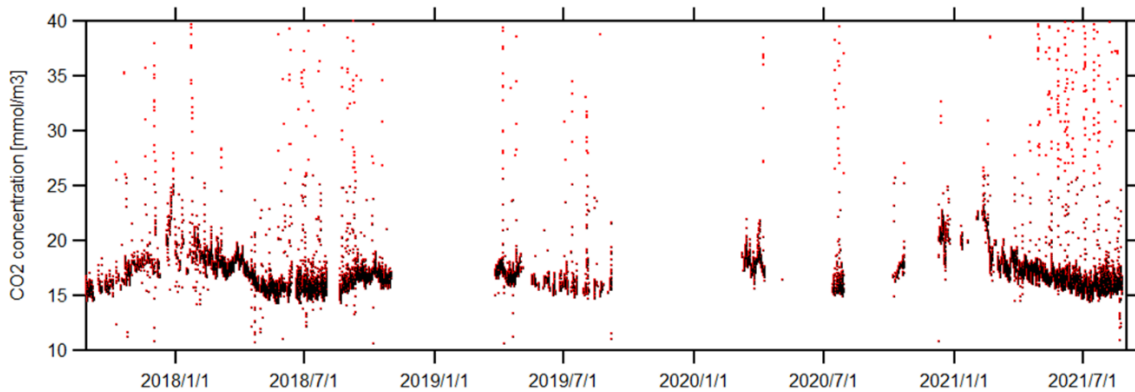


Figure 3.8: Raw data of CO₂ concentration (red dots) and data with outliers removed of CO₂ concentration (black dots) from August 2017 to August 2021.

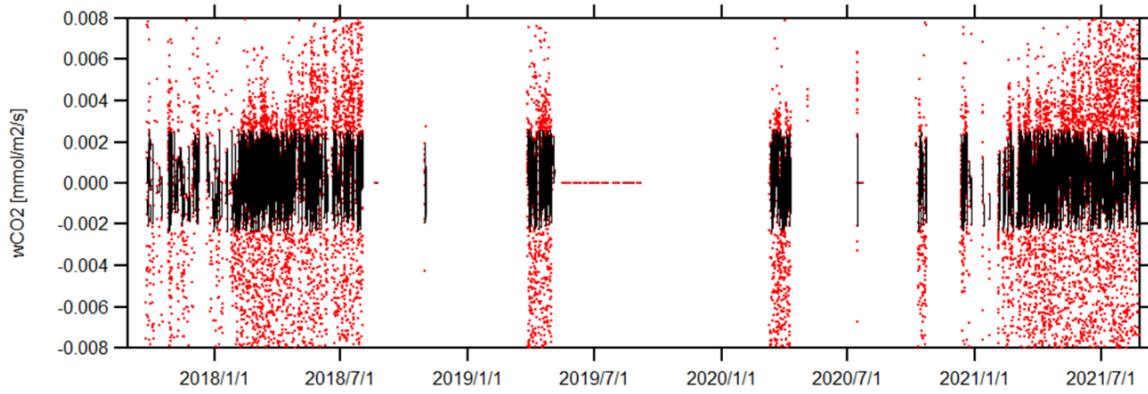


Figure 3.9: Raw data of CO₂ flux (red dots) and data with outliers removed of CO₂ flux (black dots) from August 2017 to August 2021.

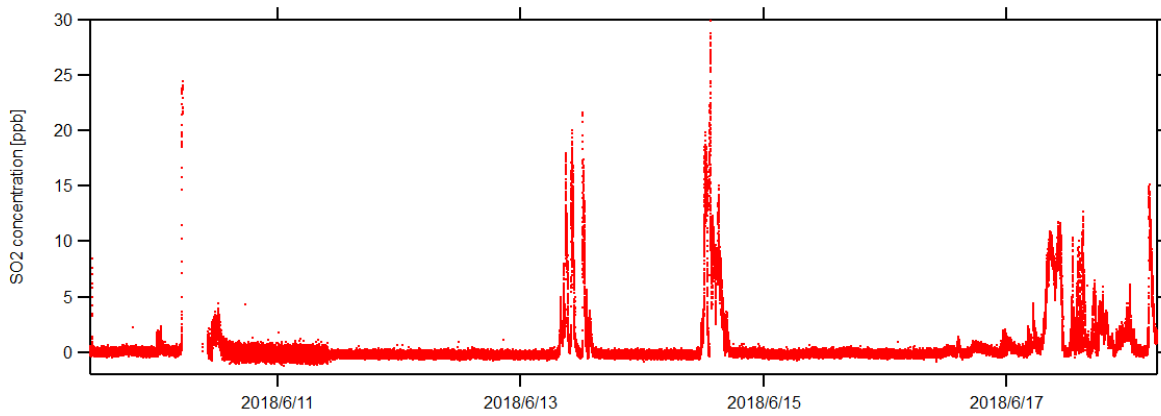


Figure 3.10: Data of SO₂ concentration from June 10th to 17th, 2018.

3.6 Selection for Yearly Comparisons

This project selected four periods from 2018, 2019, 2020, and 2021, between March 26 and April 10 each year. Because of the lack of sunlight in winter, the data for the winter months from December to February were missing for all years (see Fig. 3.7 and 3.8). The equipment on the YAJP tower normally resumes operation in March (when there is adequate sunlight), so the data from March to April was chosen for year-to-year comparison. The 16-day data from March 26th to April 10th was selected every year because the 16-day data for 2018, 2019, 2020, and 2021 are complete. Although the data for 2018 is from January to August, the data for 2017 only starts from August to December. In 2019, there are only data for March, April, July, and September, and for 2020, there are only March and April. In this way, the data from March 26th to April 10th each year were more complete than other months. So data from March 26th to April 10th every year are compared.

3.7 Analysis Methodology

This project first determined that the research objective was to study the exchange of CO₂ at the YAJP site. First, the relevant literature was reviewed to determine that temperature, water vapour, and light intensity affect the uptake and release of CO₂ by forests. CO₂ exchanges in boreal forests with other studies were compared to find out how YAJP forests differ from other forests and why. Secondly, data from instruments on the YAJP tower were collected, including the wind speed measured by the anemometer, the CO₂ concentration, CO₂ flux and H₂O concentration measured by the CO₂ and H₂O analyzer, the photosynthetically active radiation measured by the light sensors, and the temperature measured by the thermometer (data collection was from 2017 to 2021). The SO₂ concentration was measured on a Thermo Scientific model 43i (data collected for two weeks in the summer of 2018). This project used the eddy covariance method to measure the CO₂ concentration and flux, temperature and water vapor every half an hour, and then use the standard deviation method to remove the outliers caused by weather or instrument error.

The average value of various data of 15 days selected each year was calculated, and the annual trend of the average value of each data was summarized. The CO₂ concentration was then compared with temperature, H₂O concentration, and light intensity. The CO₂ flux was compared with temperature, H₂O concentration, and light intensity. Their correlations were found and it was determined which factor had a greater impact on CO₂ exchange (comparison results in Chapter 4). The monthly averages of the CO₂ concentration and CO₂ flux data measured from 2017 to 2021 were compared to find out their changing trends.

The spectrum, $S(f)$, of a variable (i.e., u) is calculated by a magnitude squared FFT of the time series, as shown in subsection 4.1. The exchange of CO₂ between the forest canopy and the atmosphere fluctuates in the time series, and there is wind shear, creating turbulence. The Fast Fourier transform (FFT) algorithm is a convenient and quick way to calculate the Fourier energy spectrum of a turbulent flow. In this project, the turbulent energy spectrum

was produced by the data measured by the anemometer and the CO₂ gas analyzer, which can analyze the structure, local isotropy and dissipation rate of the turbulent spectrum above and below the forest canopy. It can be used to observe the characteristics of CO₂ exchange between the canopy and the atmosphere.

The CO₂ concentration and CO₂ flux data for the time period selected for this project were measured while the temperature and water vapour concentration were continuously changing. The CO₂ concentration and CO₂ flux measured by the YAJP tower were compared with those measured by the CLM5.0 model under stable conditions (T=20°, RH=50%). The values of temperature and water vapour concentration measured by the YAJP tower were also substituted into the CLM5.0 model to compare the difference between the calculated CO₂ flux and the CO₂ flux measured by the YAJP tower.

The wind direction measured by the YAJP tower and the SO₂ concentration, CO₂ concentration and CO₂ flux corresponding to each wind direction were summarized. Each 20-degree wind direction was divided into an interval, and the average value of SO₂ concentration, CO₂ concentration, and CO₂ flux in each interval was calculated, and judged the change trend, and determined the wind direction interval with high concentration and flux. The relationship between wind direction and CO₂ concentration and SO₂ concentration was compared. Wind directions with high CO₂ and SO₂ concentrations were detected, and this procedure was used to determine the direction of the pollutants and which oil sands processing facilities the pollutants came from. In addition, CO₂ fluxes with and without contaminant wind directions were compared to determine whether the oil sands processing facility could affect CO₂ exchange in the forest at the YAJP site.

4. Result

4.1 Energy spectra

Flux spectra measures CO₂ exchange caused by turbulence. Figure 4.1 shows the CO₂ flux spectrum at a height of 31m. The flux spectrum should have a slope of approximately $f^{-5/3}$ in the inertial sub-range. This spectrum shows that we are sampling at a high enough frequency to capture the inertial subrange, which means we are measuring all the exchanges caused by turbulent eddies. The spectra graph in this section show that 10 Hz is a high enough frequency to capture the CO₂ exchange due to turbulence.

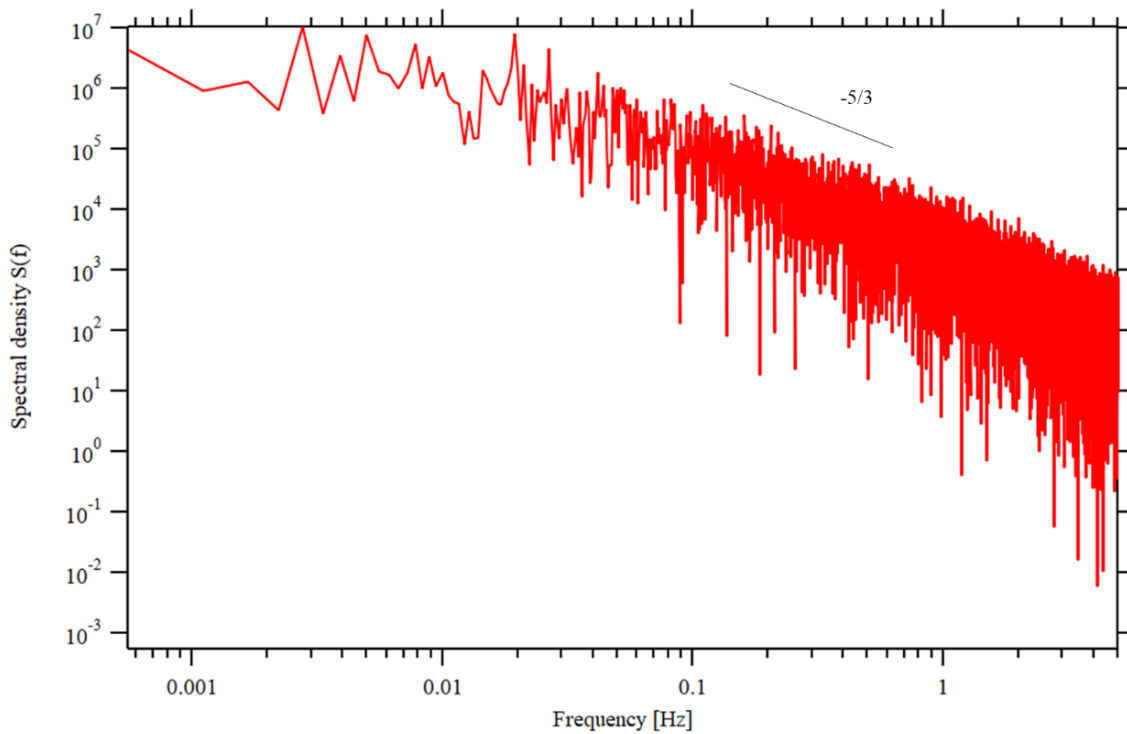


Figure 4.1: CO₂ flux spectrum at a height of 31 m in 2018.

4.2 Monthly average

By summarizing the monthly average data of CO₂ concentration and CO₂ flux, the annual variation of CO₂ concentration and flux at the YAJP site can be analyzed. The summer temperature at the YAJP site is usually 20°C to 25°C. The temperature in winter is generally between -5°C and -29°C, with the lowest temperature from January to February. Because of the lack of sunlight in winter, the YAJP tower has difficulty working under solar power, so most of the winter data is missing from the data.

Figure 4.2 shows the average monthly CO₂ concentration using five years of data. Figure 4.3 shows the average CO₂ flux with standard deviation for each month using five years of data. This shows that in the spring months of March and April, vegetation absorbs CO₂ to provide energy for life activities. Therefore, the CO₂ concentration in the air in March and April is lower than that in January and February in winter. But because the temperature in spring is still not as high as in summer, even if the light increases, the amount of CO₂ absorbed by vegetation in spring is still less than in summer. As can be seen in Figure 4.2, in summer (May to July), because the light intensity increases and the temperature increases, the life activities of plants during this period are stronger than those in spring, so the carbon dioxide concentration in the air decreases. However, the transpiration of plants themselves also increase in summer, which leads to the fluctuation of CO₂ concentration in Figure 4.2, and the value of CO₂ flux in Figure 4.3 also peaks in May. In autumn (August to October in Figure 4.2), plant photosynthesis weakens and trees stop growing, resulting in an increase in CO₂ concentration in the air and a gradual decrease in CO₂ flux (Figure 4.3). In Fig. 4.2, the air CO₂ concentration in winter (November to January) is the highest in the whole year, and the value of CO₂ flux is also close to zero, or even greater than zero (Fig. 4.3).

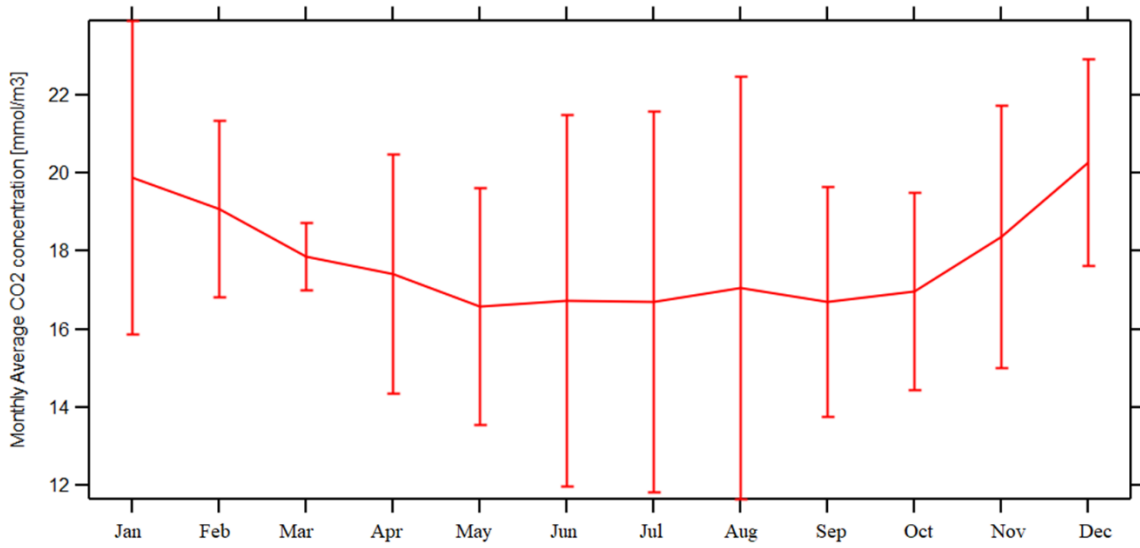


Figure 4.2: The average CO₂ concentration for each month from 2017, 2018, 2019, 2020, and 2021.

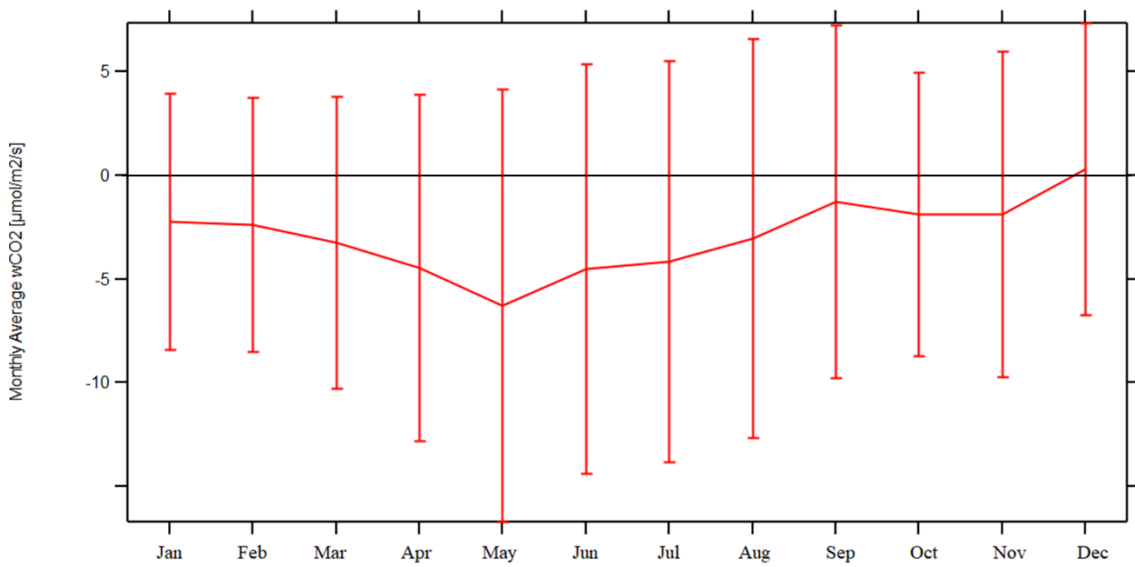


Figure 4.3: The average CO₂ flux for each month with standard deviations from 2017, 2018, 2019, 2020, and 2021.

4.3 Wind Direction Description

This project discusses the effect of wind direction on CO₂, so the frequency of occurrence of all wind directions is summarized here. Figure 4.4 shows the wind direction summary at the height of 31m from 2017 to 2021. In the figure, it can be seen that there are more winds in the wind direction of 320 to 20 degrees, and 100 to 175 degrees. There are relatively few winds between 30 and 70 degrees.

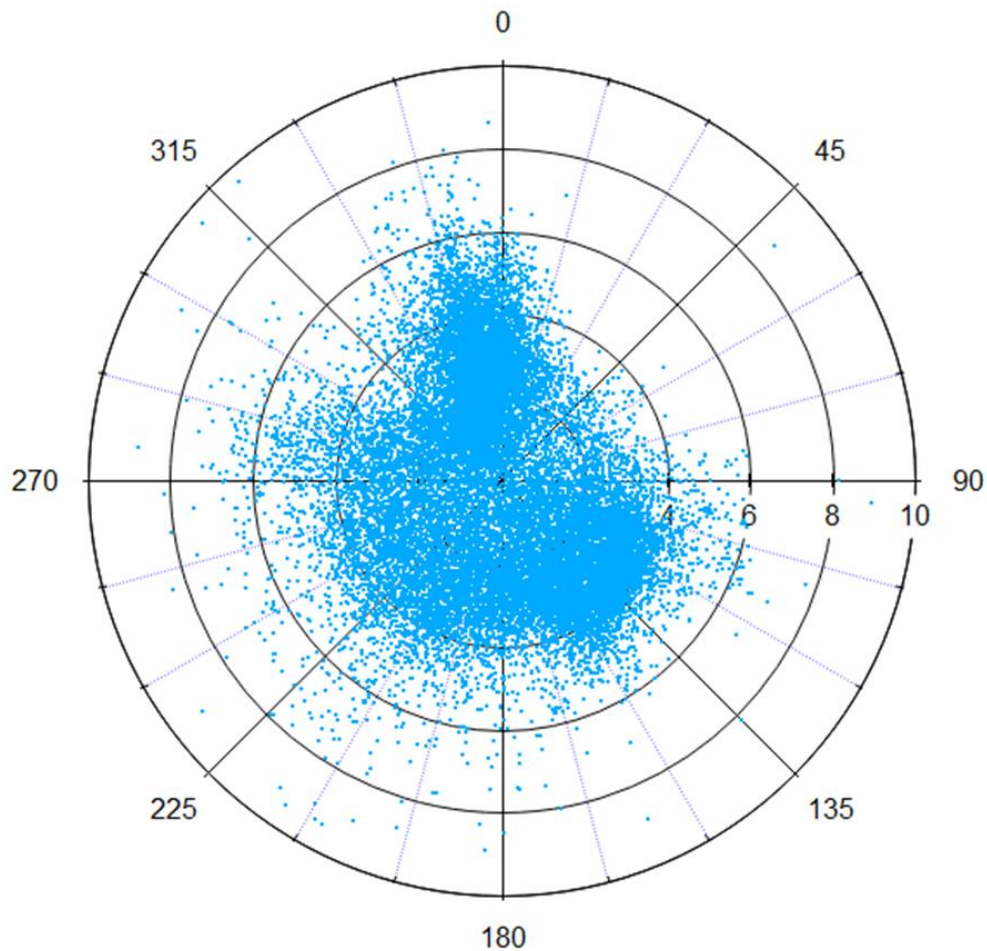


Figure 4.4: The relationship between wind direction and wind speed (m/s) at the height of 31m from 2017 to 2021.

4.4 Analysis of Temperature from Sonic anemometer

Changes in temperature affect the exchange of CO₂. This section summarized the change in temperature for selected time periods from 2018 to 2021. Figure 4.5 shows the temperature trend from March 26 to April 10, 2018 to 2021. In 2018 from March 26 to April 10, the average temperature at a height of 31 meters was -6.3°C, and the average temperature at a height of 5 meters was -5.2°C. In 2019 at the same time, the average temperature at 31 meters has risen to -0.4°C. But by 2020, it has dropped to -3.6°C. The average temperature at 5 meters in 2020 has increased to -1.8°C compared with 2018. From March 26 to April 10 in 2021, the average temperature at 31 meters in the area rose to 5.1°C. Compared with previous years, the temperature has changed to a positive value, and it has risen by approximately 8 degrees compared to 2020.

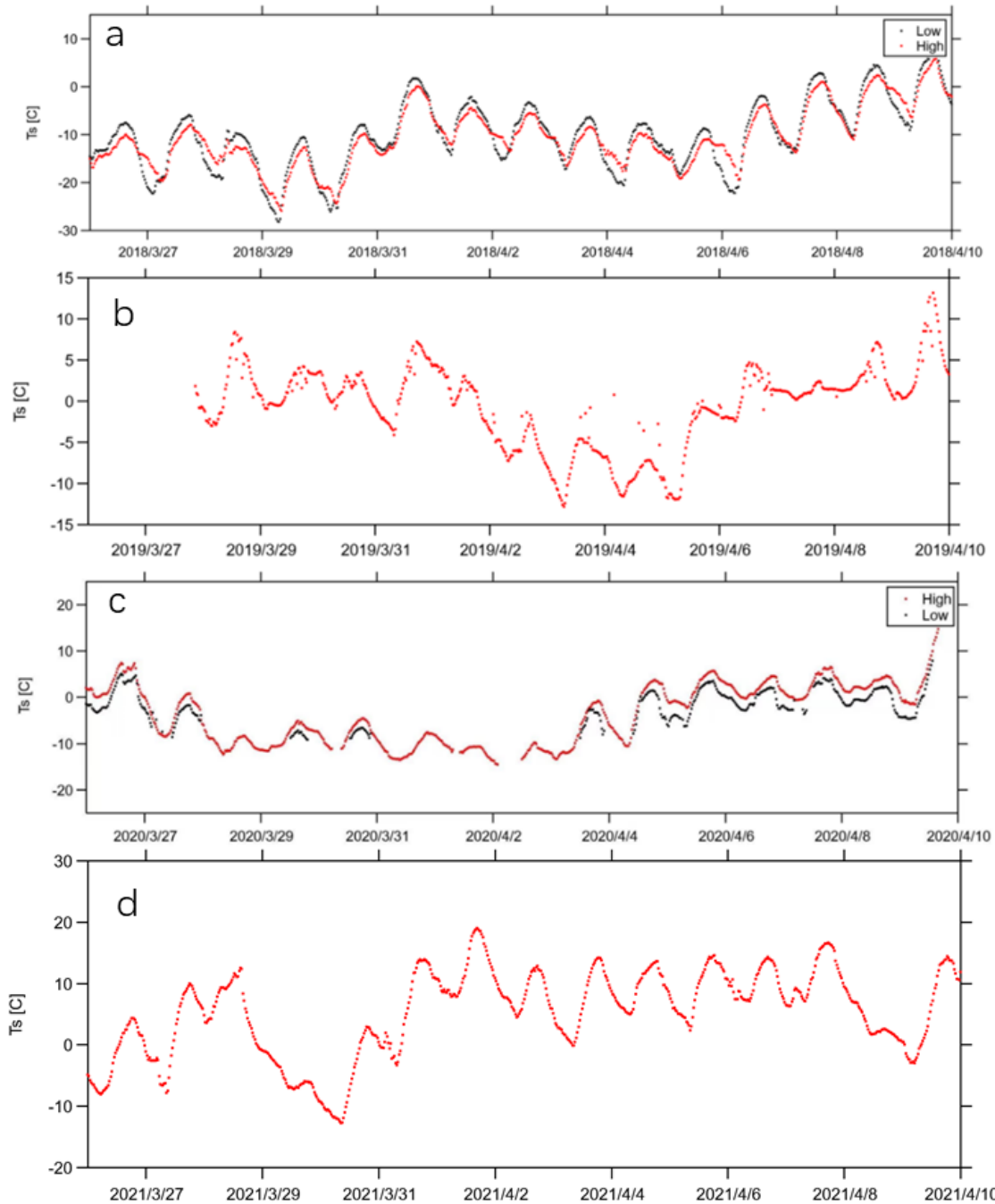


Figure 4.5: Temperature data from Sonic anemometer s at 31 m (High) and 5 m (Low). (a): temperature data in 2018. (b): temperature data in 2019. (c): temperature data in 2020. (d): temperature data in 2021. The temperature data at a height of 5 meters was not recorded in March and April 2019 and 2021. Data were measured by YAJP tower.

4.5 Analysis of water vapour

The growth of vegetation needs water, and the water vapour in the air will also affect the photosynthesis of the vegetation, so it is very important to study the exchanges of water vapour concentration in the air. Figure 4.6 shows the change trend of water vapour concentration from March 26 to April 10, 2018 to 2021. The average value of water vapour concentration was 177.9 mmol/m³ in 2018. This increased to 291.9 mmol/m³ in 2019, and decreased to 227.2 mmol/m³ in 2020. The latest data in 2021 shows that the average value of water vapour concentration has increased to 253.8 mmol/m³.

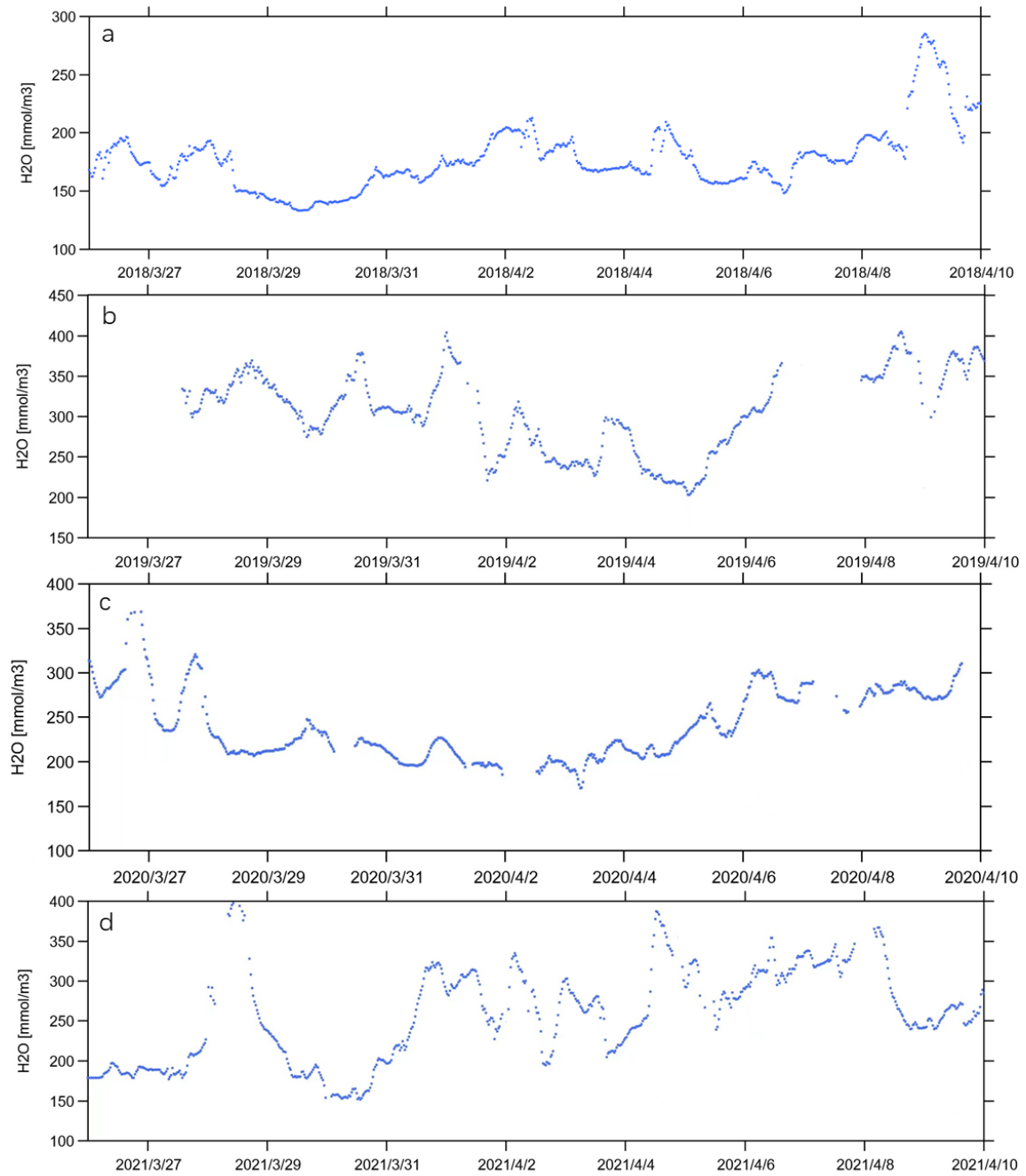


Figure 4.6: (a): H₂O data in 2018. (b): H₂O data in 2019. (c): H₂O data in 2020. (d): H₂O data in 2021. Data were measured by YAJP tower.

4.6 CO₂ concentration

Changes in temperature, H₂O, and pollutants released by surrounding oil processing and extraction may cause changes in the CO₂ concentration during the test period. According to the CO₂ concentration data measured by the YAJP tower at height of 31 m, the CO₂ concentration in the air showed a downward trend in the two weeks of March/April in 2018, 2019, and 2020. It can be seen from Figure 4.7, it dropped from 17.8 mmol/m³ in March/April 2018 to 17.4 mmol/m³ in March/April 2019, and finally to 15.9 mmol/m³ in March/April 2020. But by 2021, the average CO₂ concentration in March/April was 17.3 mmol/m³. Compared with 2020, the average CO₂ concentration has increased by 1.4 mmol/m³.

March to April is spring, with plenty of sunlight. The intensity of sunlight affects the growth of plants. Adequate sunlight in spring provides plants with the ability to carry out various life activities. Increased light intensity will increase the temperature and vegetation will absorb more CO₂, so the CO₂ in the air will decrease. When winter ends and spring begins, the heat generated by the increased sunlight will melt the snow on the ground. Strong sunlight will increase the humidity in the air and increase the photosynthesis of vegetation, which will absorb more CO₂, as shown in equation R1 in section 2.1.2. It can be found in the Figures 4.7.1 - 4.7.4 that when the temperature increased, the concentration of CO₂ in the air decreased, when the temperature decreased, the concentration of CO₂ in the air increased. It also can be seen that when the concentration of water vapour concentration increased, the concentration of CO₂ in the air also decreased.

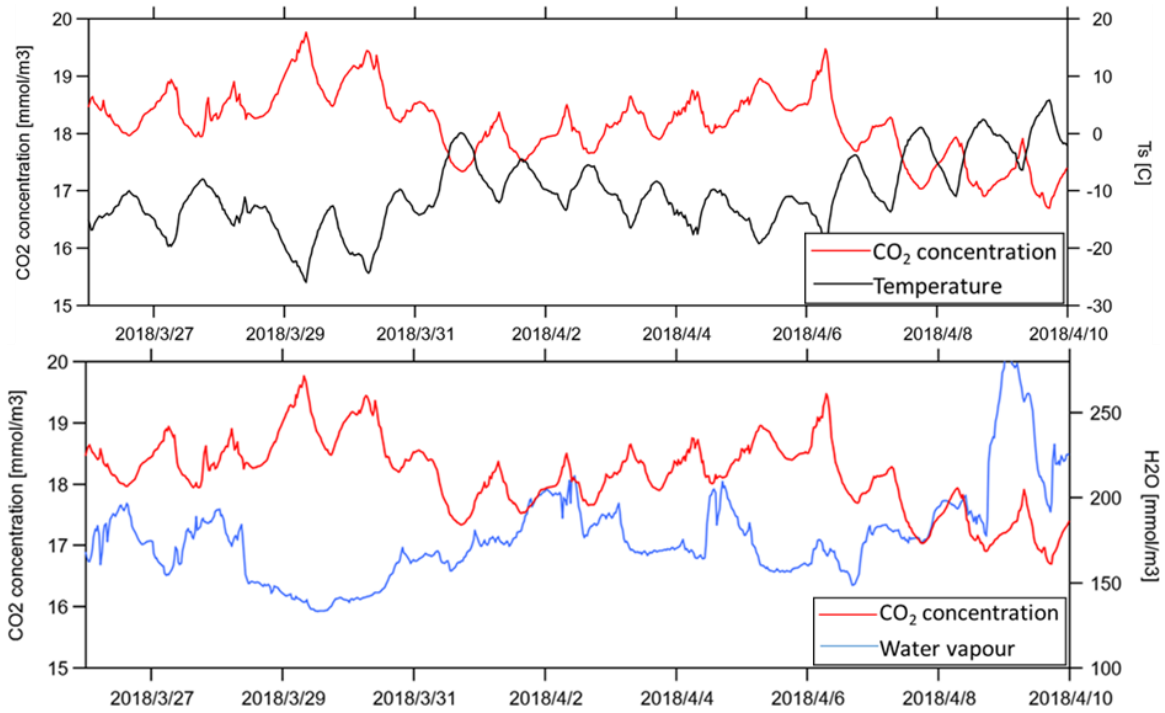


Figure 4.7.1: The relationship between CO₂ concentration (red lines) and temperature (black line) and water concentration (blue line) in 2018. Data were measured by YAJP tower.

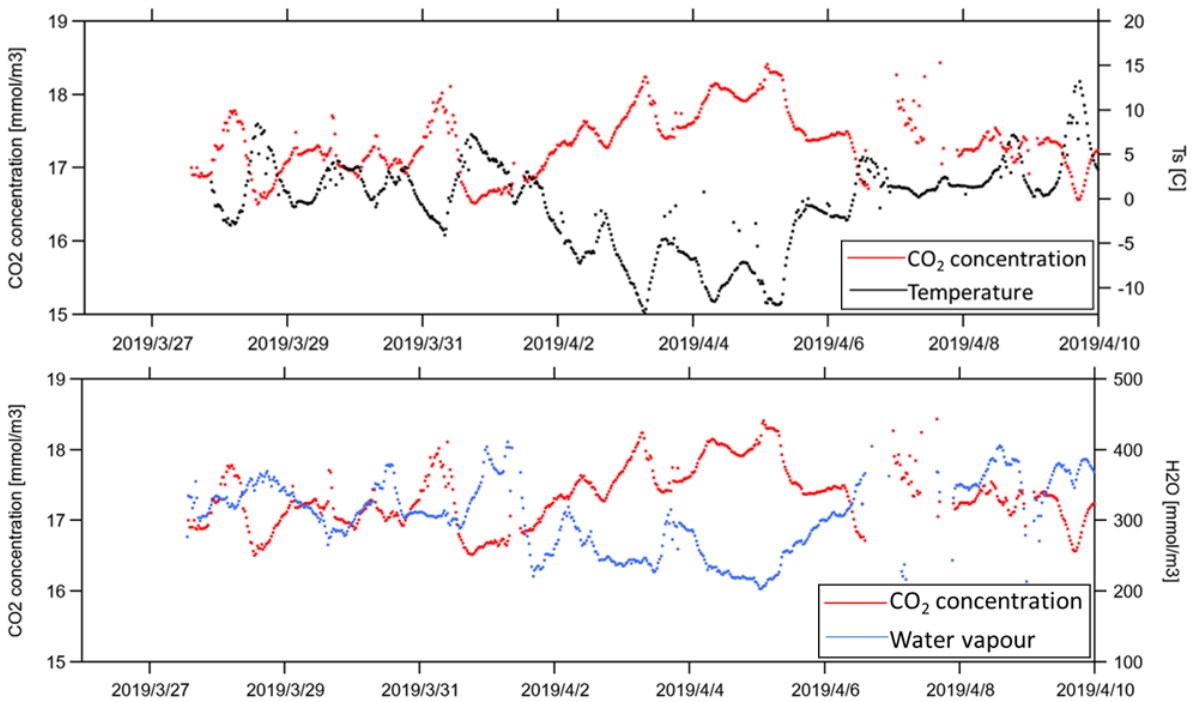


Figure 4.7.2: As Figure 4.7.1 for 2019.

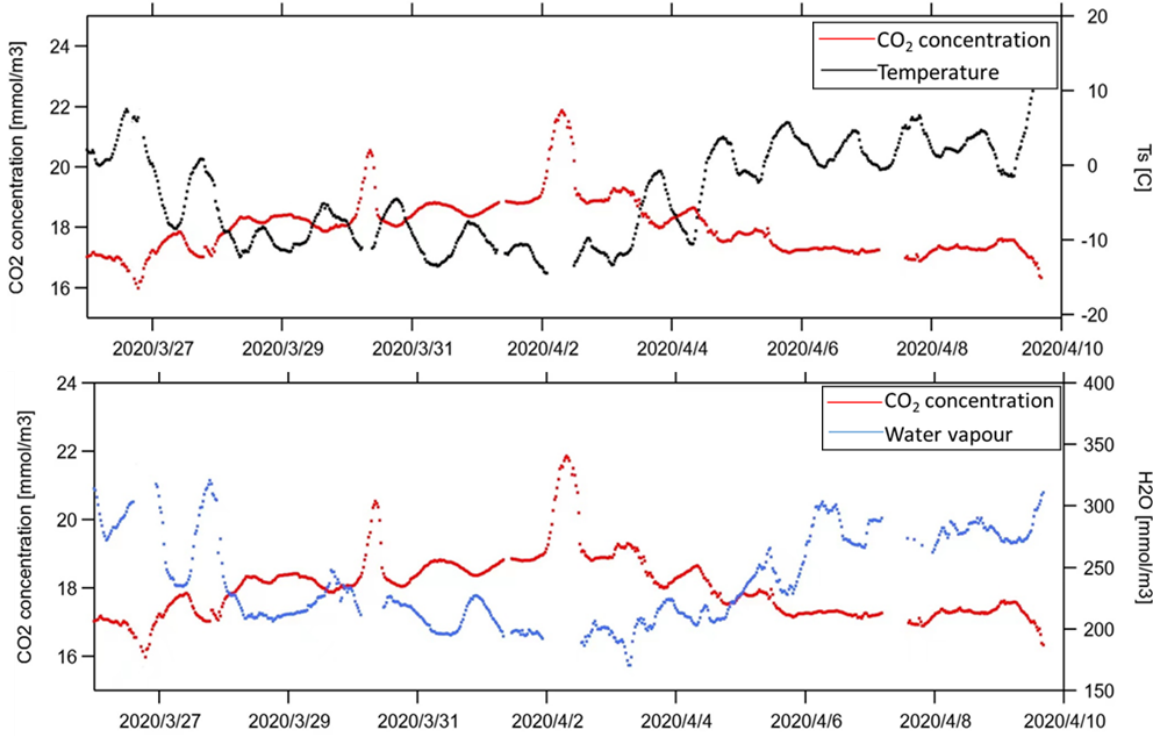


Figure 4.7.3: As Figure 4.7.1 for 2020.

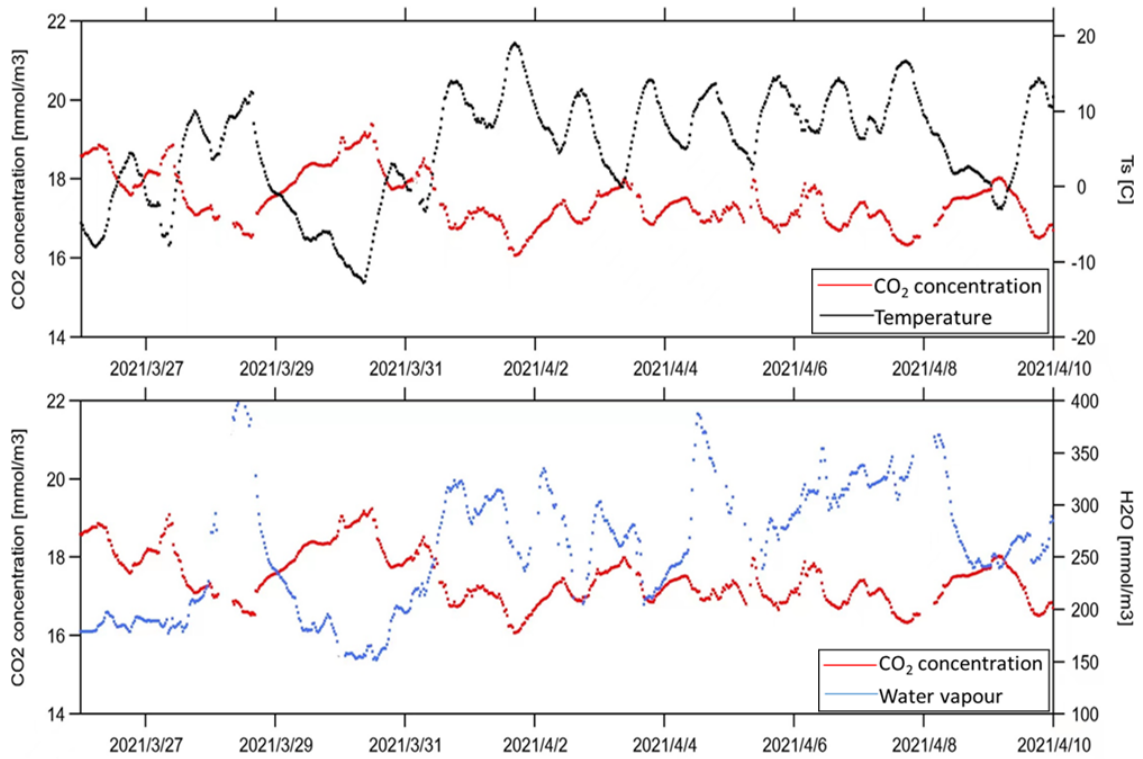


Figure 4.7.4: As Figure 4.7.1 for 2021.

4.7 CO₂ flux

The average CO₂ flux values in four selected time periods are negative, which means that the forest was a net absorber of CO₂ from the atmosphere. In 2018, the net CO₂ flux for this 15-day period was -4.3 μmol/m²/s, increasing to -2.3 μmol/m²/s in 2019, then slightly declining to -2.4 μmol/m²/s in 2020. By March/April in 2021, the average value of CO₂ flux has dropped to -2.7 μmol/m²/s.

Like the CO₂ concentration, sufficient light will increase the water vapour and temperature in the air. It will strengthen the photosynthesis of vegetation, causing vegetation to absorb more air CO₂. Therefore, CO₂ is transferred from the air to the forest, so the value of CO₂ flux is negative.

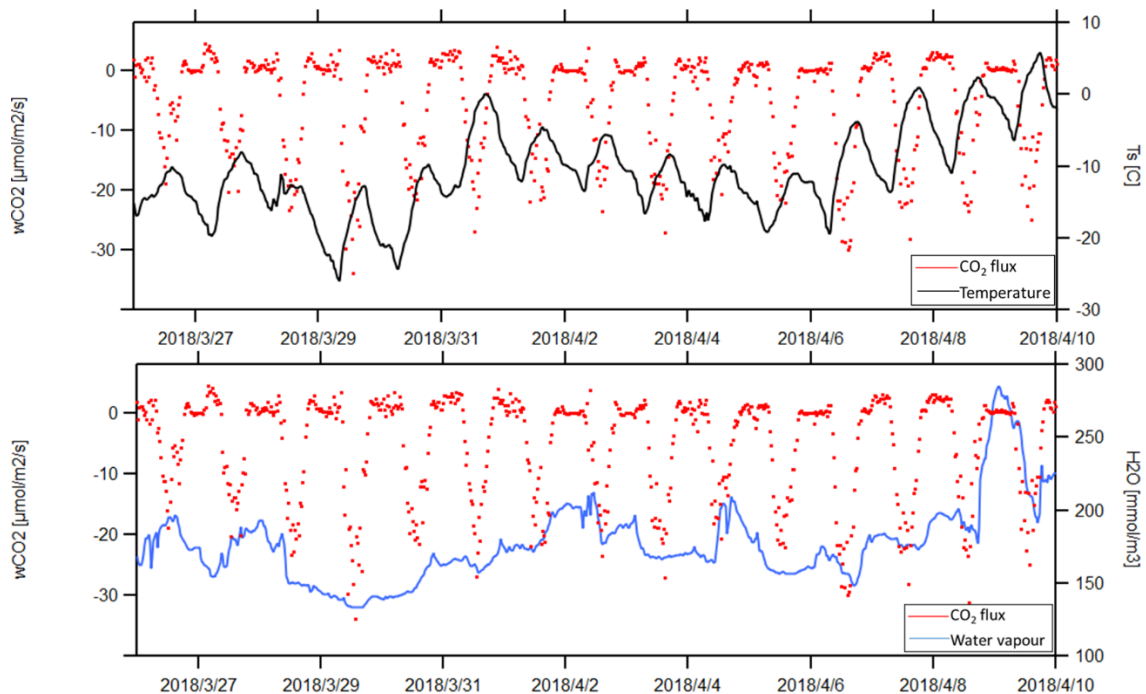


Figure 4.8.1: The relationship between CO₂ flux and temperature and water concentration in 2018. Data were measured by YAJP tower.

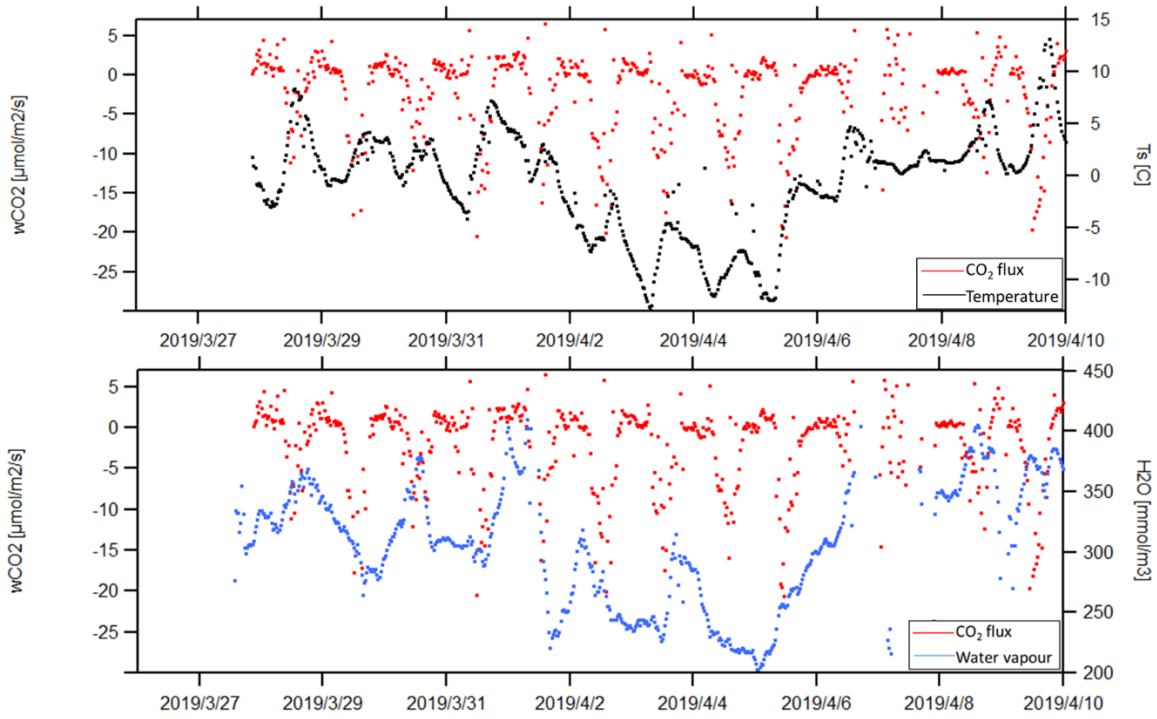


Figure 4.8.2: As Figure 4.8.1 for 2019.

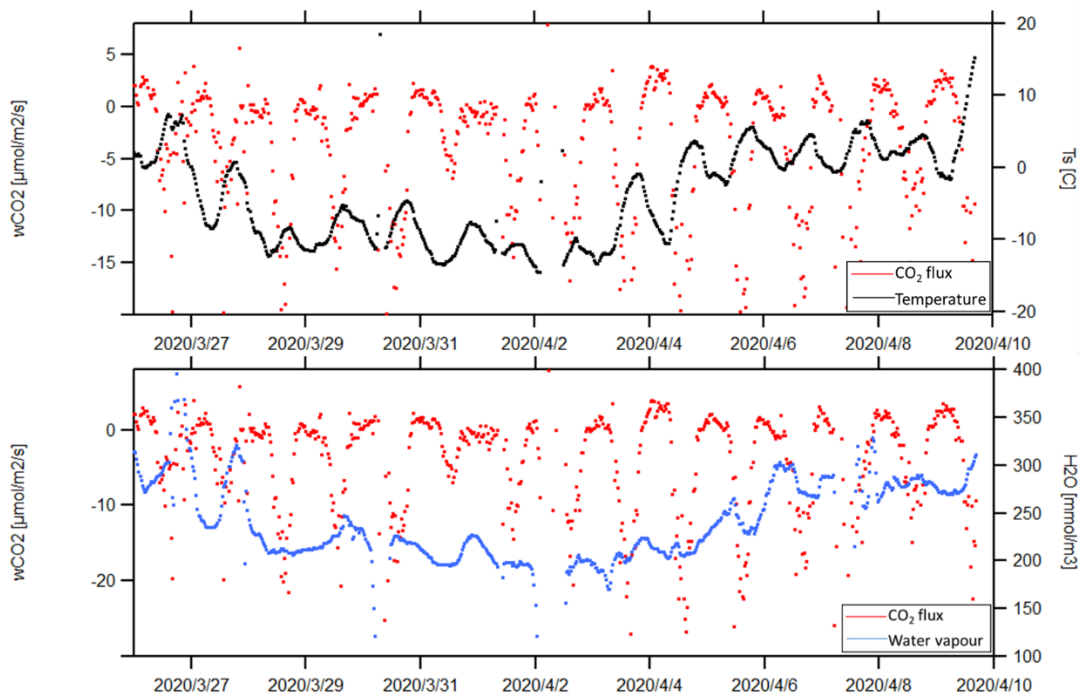


Figure 4.8.3: As Figure 4.8.1 for 2020.

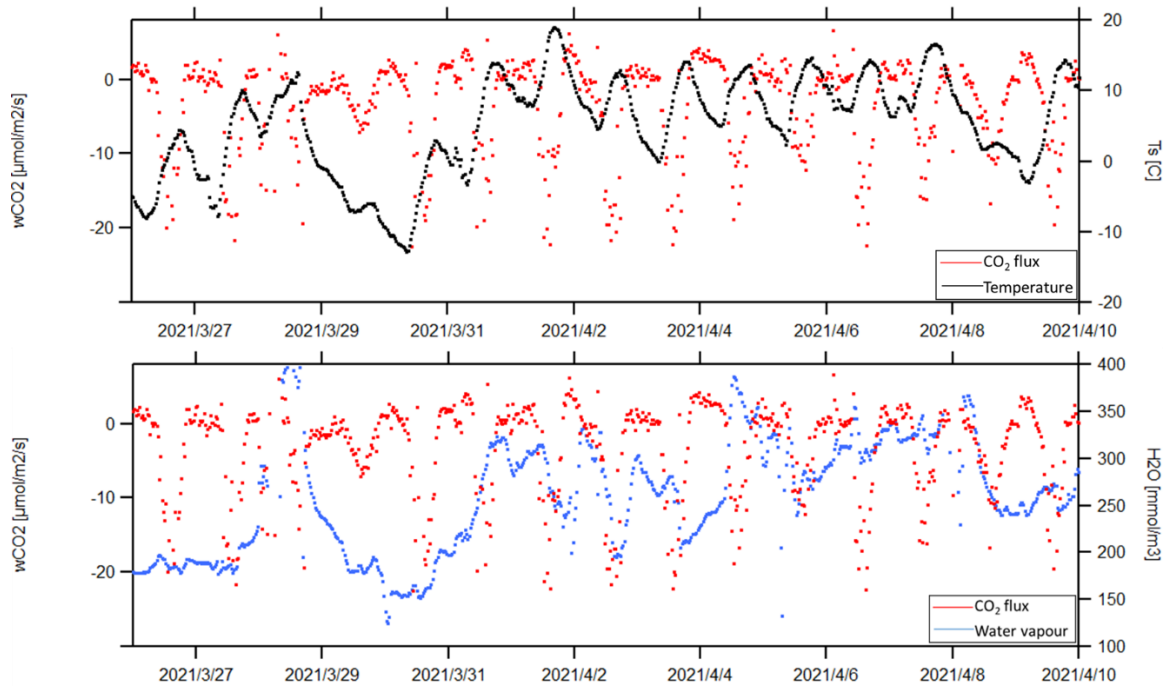


Figure 4.8.4: As Figure 4.8.1 for 2021.

4.8 Photosynthetically Active Radiation (PAR)

The intensity of sunlight affects the absorption of CO₂ by vegetation. Figure 4.9 shows the change in photosynthetically active radiation from March 26 to April 10 from 2018 to 2021. Photosynthetically active radiation in March/April was 363 $\mu\text{mol}/\text{m}^2/\text{s}$ in 2018, 217 $\mu\text{mol}/\text{m}^2/\text{s}$ in 2019, 238 $\mu\text{mol}/\text{m}^2/\text{s}$ in 2020, and 273 $\mu\text{mol}/\text{m}^2/\text{s}$ in 2021.

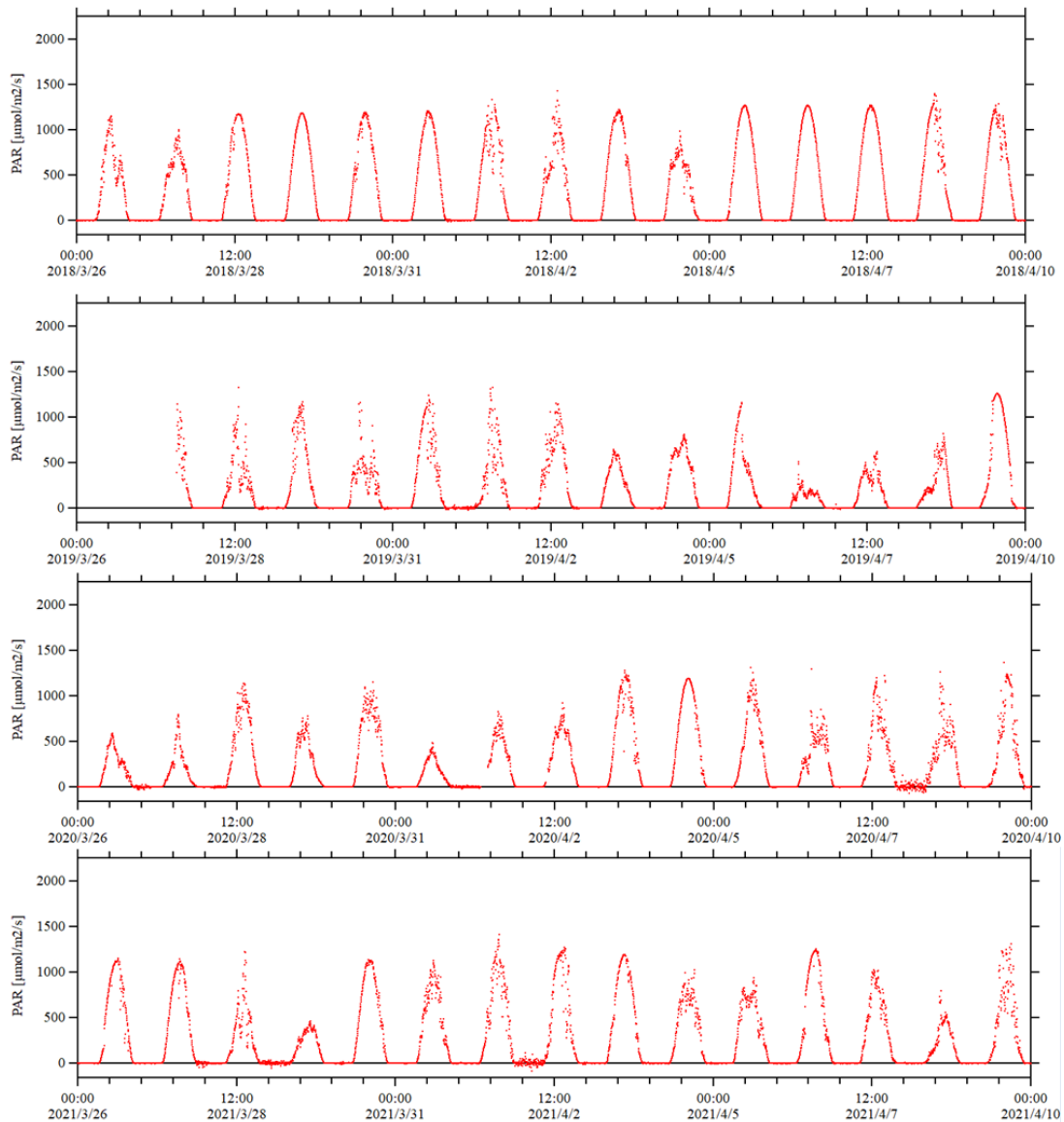


Figure 4.9: Photosynthetically Active Radiation (PAR) in 2018 to 2021. Data were measured by YAJP tower.

4.9 CO₂ flux calculated by the CLM model

This project used the CLM5.0 model to roughly calculate the CO₂ flux value for a specified weather conditions but did not run the entire model for an extended period. The CO₂ flux values obtained by these rough calculations are compared with the data measured by the YAJP tower.

As discussed in Section 2.6, CO₂ flux can be calculated using the formula (5).

According to Eq. 5, with $c_s/P_{atm} = C_{CO_2}$, combining formula (3) and formula (5) gives:

$$F = m_{CO_2} L C_{CO_2} \left[g_0 + 1.6 \left(1 + \frac{g_1}{\sqrt{D}} \right) \frac{A_n}{C_{CO_2}} \right] \quad (17)$$

where $g_0 = 100 \mu\text{mol/m}^2/\text{s}$, $g_1 = 2.35 \mu\text{mol/m}^2/\text{s}$ (from the CLM 5.0 website: https://escomp.github.io/ctsm-docs/versions/release_clm5.0/html/tech_note/index.html), the LAI $L = 2$, $m_{CO_2} = 44.01 \text{ g/mol}$. The vapour pressure deficit (D) at the leaf surface (kPa) is calculated from

$$e_s = A \exp \left(-\frac{B}{T} \right) \quad (18)$$

$$RH = f = \frac{e}{e_s} \quad (19)$$

$$D = e_s - e \quad (20)$$

where $RH = f$ is relative humidity, $A = 2.53 \times 10^{11} \text{ Pa}$ is C-C Eq. constant for water vapour, $B = 5420 \text{ K}$ is C-C Eq. constant for water vapour, T (K) is air temperature, e (Pa) is vapour pressure, e_s (Pa) is saturation vapour pressure. Here we assume $A_n \approx 10 \mu\text{mol/m}^2/\text{s}$, which is typical for a sunny summer afternoon (Thornley, 1998).

Using these values, when the weather is very sunny, the temperature is 20° and the humidity is 50%, the final CO₂ flux (F) is -16 $\mu\text{mol/m}^2/\text{s}$.

4.10 CO₂ concentration and SO₂ concentration with wind direction

After summarized the wind direction, we need to compare the wind direction with the corresponding CO₂ concentration, CO₂ flux and SO₂ concentration. Near the YAJP site, there are mainly south-southwest winds and north-northeast winds (Jiang, 2018, and shown in Figure 4.4). Figure 4.10 shows the relationship between CO₂ concentration, CO₂ flux, SO₂ concentration and wind direction. Each bin represents the mean value of a 20 degrees wind direction interval.

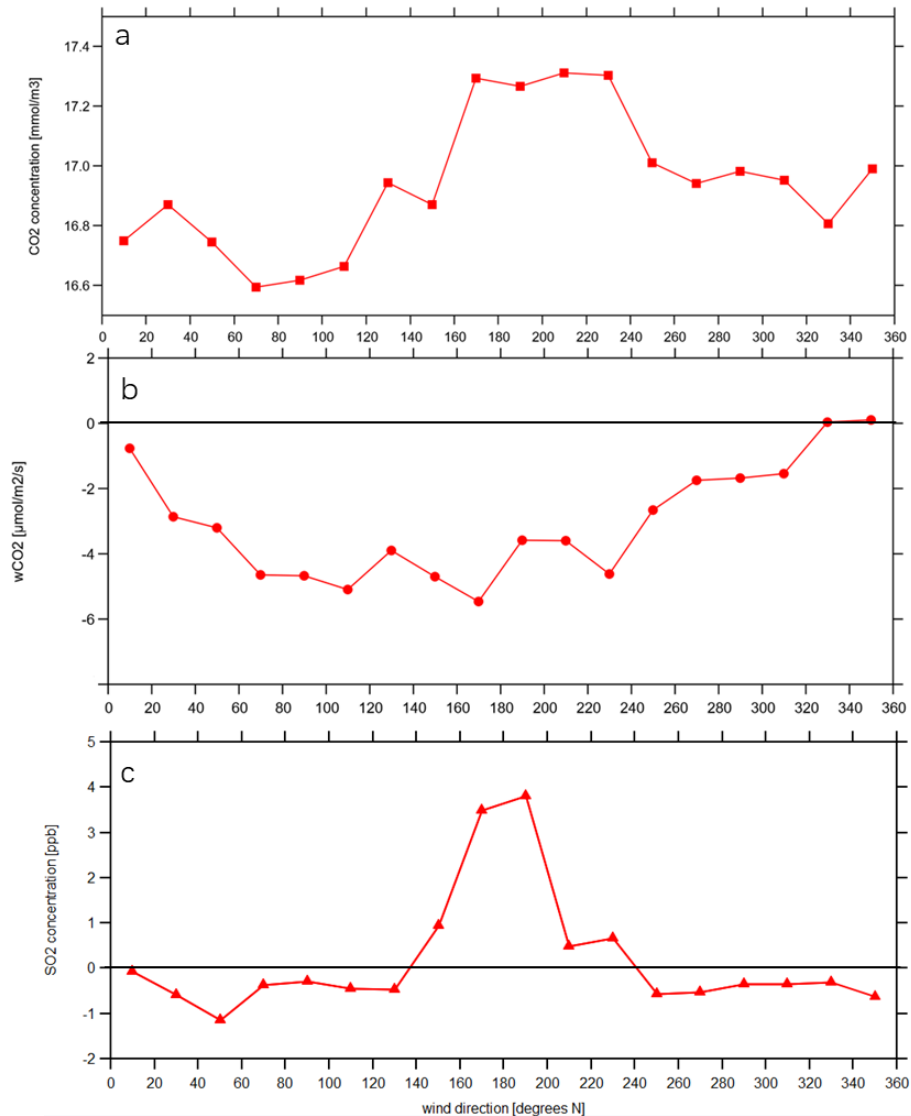


Figure 4.10: (a): Average CO₂ concentrations with wind direction from August 2018 to July 2020. (b): Average CO₂ fluxes with wind direction from August 2018 to July 2020. (c): Average SO₂ concentrations with wind direction from June 10 to 17, 2018.

As shown in Figure 4.10, for wind directions between 170 degrees and 230 degrees, the CO₂ concentration measured at the YAJP tower was relatively high (Figure 4.10a), and when the wind direction was between 170 degrees and 200 degrees, the SO₂ concentration was relatively high at YAJP site (Figure 4.10c). The negative SO₂ concentration in the measured data is due to an instrument error because the Thermo Sci instrument was not properly calibrated for low concentrations. But the project only focused on the direction of the plume, so this error does not affect the conclusions about the wind direction.

Higher CO₂ concentrations were also observed in wind directions outside of 170° to 230°. The reason for this is that the development of oil sands facilities includes not only smokestacks, but also mining, tailings storage, heavy haulage vehicles, and excavators, all of which contribute to the increased CO₂ concentrations in the air. The CO₂ flux is lower in magnitude at lower CO₂ concentrations, because the low CO₂ concentration affects the growth of plants themselves, resulting in less CO₂ uptake by plants.

The Syncrude processing facility and Suncor processing facility are both within 16 km of the YAJP forest (Fig. 4.11). These facilities have smokestacks that emit pollutants. The purpose of comparing the concentration of SO₂ with the wind direction is to find out which direction the pollutants are coming from to determine how pollution from oil facilities affects changes of CO₂ in the forest. According to the current data, we conclude that when the wind direction is around 180 degrees, the YAJP tower measured more SO₂ and CO₂. The negative wCO₂ value represents exchange of CO₂ from the atmosphere to the forest. It can be seen from the figure that the concentration of CO₂ in the atmosphere is relatively high for wind directions between 170° and 230°, and relatively low for wind directions between 70° and 110°. The concentration of SO₂ is highest in the wind direction range from 170° to 200° and is near zero from all other wind directions. The Syncrude smokestack is located at about 230 degrees from the YAJP tower, and the Suncor smokestack is located at about 190 degrees from the YAJP tower. Therefore, this indicates that both the Syncrude processing facility and the Suncor processing facility bring some pollution to the YAJP site,

and the Suncor processing facility brings more pollution to the YAJP site. This pollution seems to be associated with higher CO₂ concentration and greater uptake of CO₂ to the forest. But because there are many wind directions, not all wind directions bring pollutants to the YAJP study area.

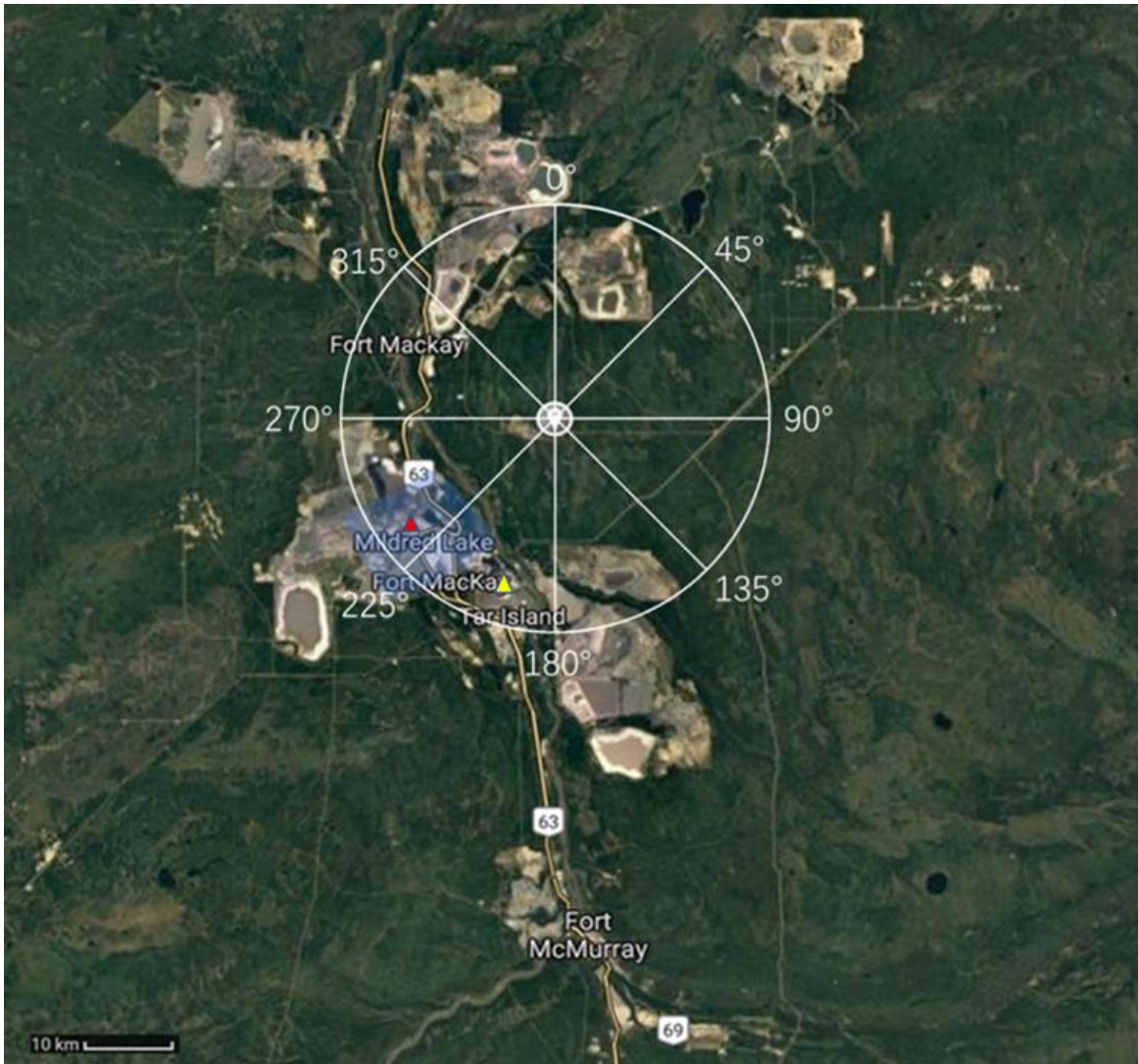


Figure 4.11: The wind direction coordinates at YAJP tower. The radius of circle is 20km. The red triangle is Syncrude stack location, and the yellow triangle is Suncor stack location.

5. Discussion

5.1 Comparison of temperature, water vapour concentration, PAR, CO₂ concentration and CO₂ flux

The temperature and water vapour concentration of 15 days in March/April of each year from 2018 to 2021 at the YAJP site (red line) are summarized, as shown in Figure 5.1. In addition, the annual average temperature and water vapour concentration values of the JP104 site (black line) in 2018, 2019, 2020 and 2021 are also shown in Figure 5.1.

At the YAJP site, the temperature is relatively high in March/April 2019 and March/April 2021, being -0.4°C and 5.1°C respectively. The water vapour concentration was the highest in March/April 2019, with 291.9 mmol/m³. And the changing trends of temperature and water vapour are similar. Compared with the JP104 site (Figure 5.1 black line), the annual average temperature of the JP104 site showed a trend of slightly decreasing and finally increasing, with a small difference from the 15-day average temperature of the YAJP site. However, the annual mean H₂O concentration at the JP104 site was higher than that at the YAJP site and increased gradually. The YAJP locations in March/April are drier.

Summarizing the data for these 15 days of each year, temperature and water vapour are negatively correlated with CO₂ concentration (Chapter 4.7), and positively correlated with CO₂ flux (Chapter 4.8). However, as shown in Figure 5.2, comparing the average value of annual changes in temperature, water vapour, CO₂ concentration and CO₂ flux, when the temperature and water vapour concentration increased, the values of CO₂ concentration and CO₂ flux were also increased. When the temperature and water vapour concentration decreased, the CO₂ concentration and CO₂ flux value also decreased.

It can be concluded that when the temperature is higher, the photosynthesis of vegetation is increased, and vegetation absorbs more CO₂ (data for 2018, 2019 and 2020 in Figure 5.2a). As shown in Figure 5.3a, when the temperature is lower, the CO₂ transferred from the atmosphere to the forest is decreased.

Similarly, water vapour in the air also affects the absorption of CO₂ by plants. When the

water vapour in the air is increased, this results in a decrease in the transfer of CO₂ from the atmosphere to the forest (Figure 5.3b) and an increased in CO₂ in the atmosphere (Figure 5.2b).

The correlation between temperature and CO₂ concentration for these 15-day averages is $R = 0.07$, and the correlation between water vapour concentration and CO₂ concentration is $R = -0.08$. The correlation between temperature and CO₂ flux is $R = 0.6$, and the correlation between water vapour concentration and CO₂ flux is $R = 0.8$.

The measured data is in spring (March/April) in each year. Although the sunlight was strong in spring, the temperature was still at or below zero, so the plant’s metabolic activity was still relatively slow in order not to be frozen (Juurola, 2016). ()

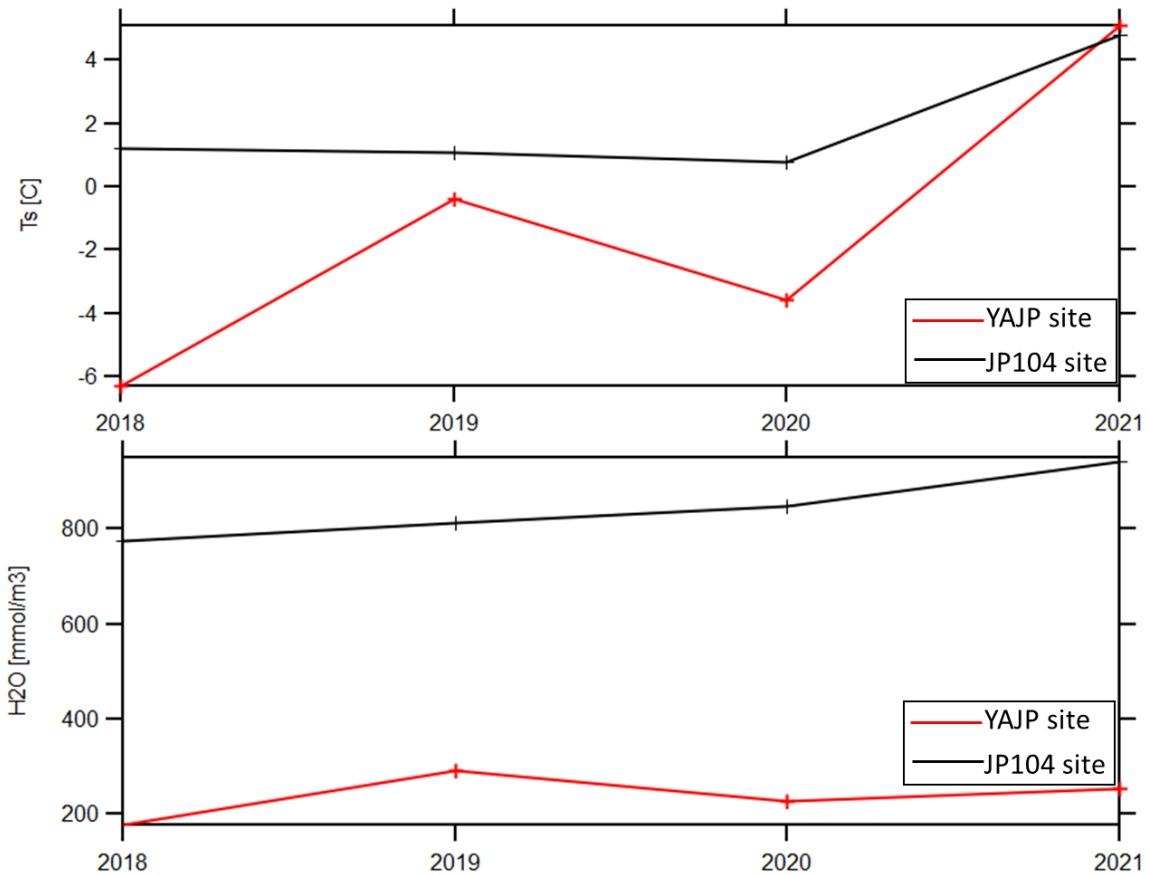


Figure 5.1: Red line is the average of temperature and water vapour concentration of 15 days in March/April of each year from 2018 to 2021 at YAJP site, black line is annual average temperature and water vapour concentration values at JP104 site.

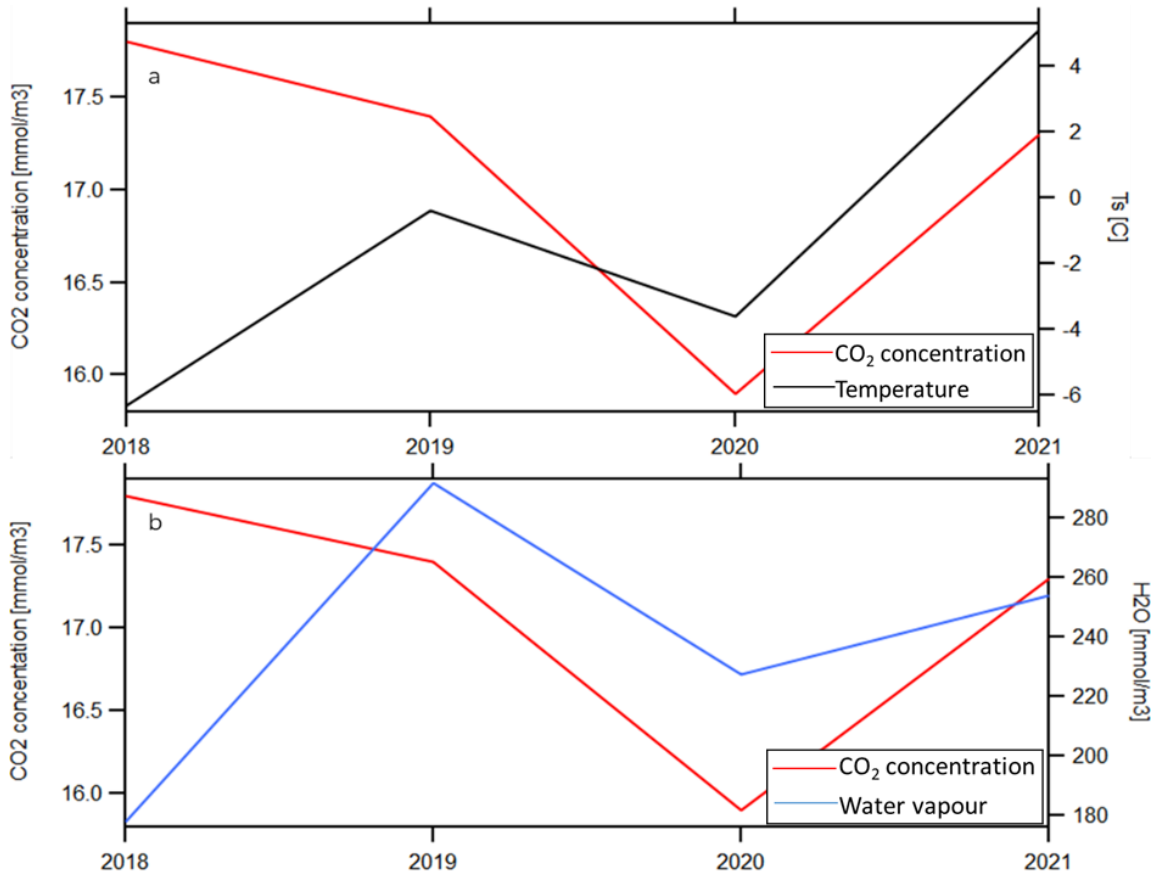


Figure 5.2: CO₂ concentration (red lines) compared with temperature (black line) and water vapour (blue line) of 15 days in March/April of each year from 2018 to 2021.

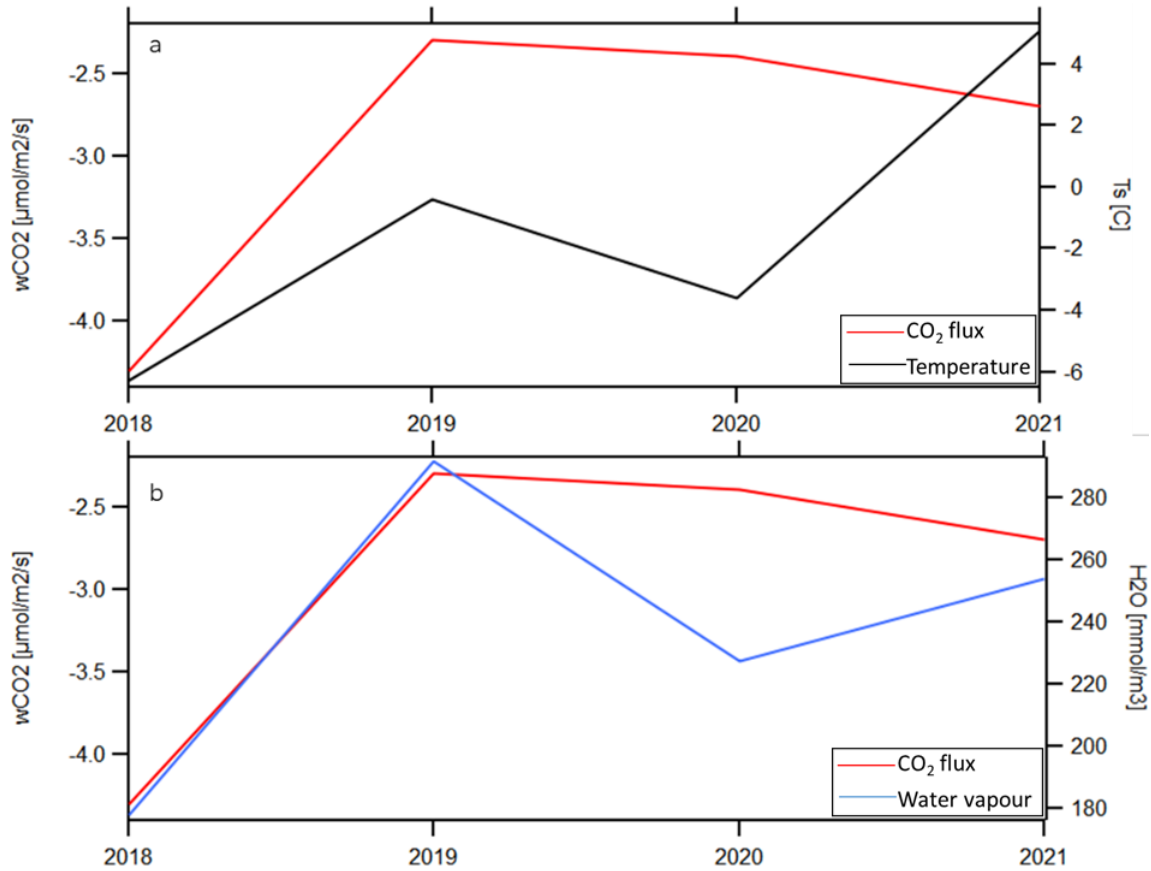


Figure 5.3: CO₂ flux (red lines) compared with temperature (black line) and water vapour (blue line) of 15 days in March/April of each year from 2018 to 2021.

Photosynthetically active radiation also effects exchanges in CO₂. Figure 5.4 shows the relationship between photosynthetically active radiation (PAR) with CO₂ concentration and CO₂ flux for 15 days. When PAR was enhanced, the CO₂ concentration in the atmosphere was lower (as shown in Figure 5.4a), and the correlation between PAR and CO₂ concentration is R=0.6. Similarly, when PAR increased, more CO₂ in the air was transferred to the forest, so the CO₂ flux increased, and the correlation between PAR and CO₂ flux was R=-0.9. Due to the high correlation between PAR and CO₂ flux, it can be demonstrated that CO₂ flux is mainly driven by photosynthesis.

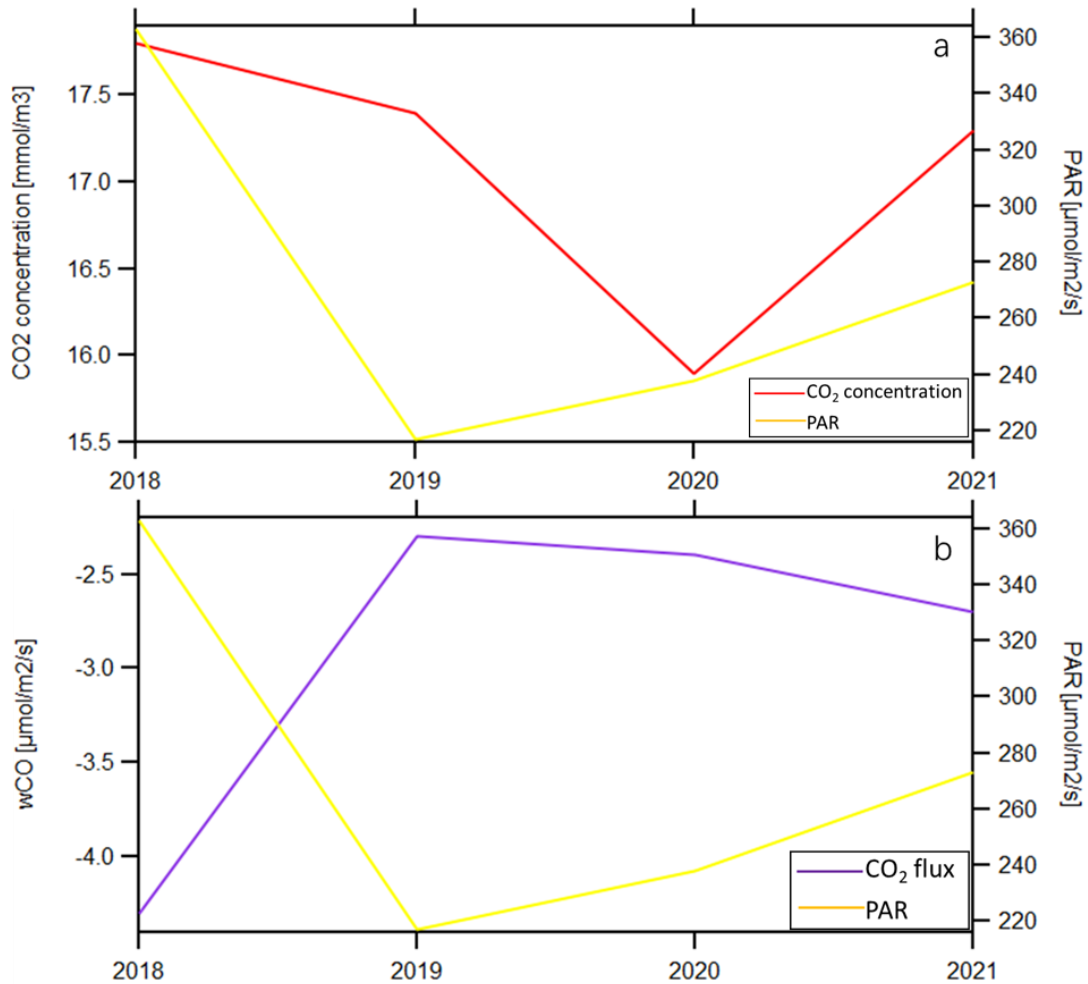


Figure 5.4: CO₂ concentration (red lines) and CO₂ flux (purple line) compared with PAR (yellow line) of 15 days in March/April of each year from 2018 to 2021.

Changes in CO₂ concentration also affect CO₂ fluxes. Comparing CO₂ concentrations and fluxes for the selected time periods from 2018 to 2021 (Figure 5.5), it was found that when CO₂ concentrations decreased, the amount of CO₂ absorbed by the forest decreased, and the exchange of CO₂ between the forest and the atmosphere decreased (e.g., data for 2018, 2019, and 2020). When the CO₂ concentration increased, more CO₂ was absorbed by the forest (e.g., data for 2021), and the correlation between CO₂ concentration and CO₂ flux is $R=-0.5$.

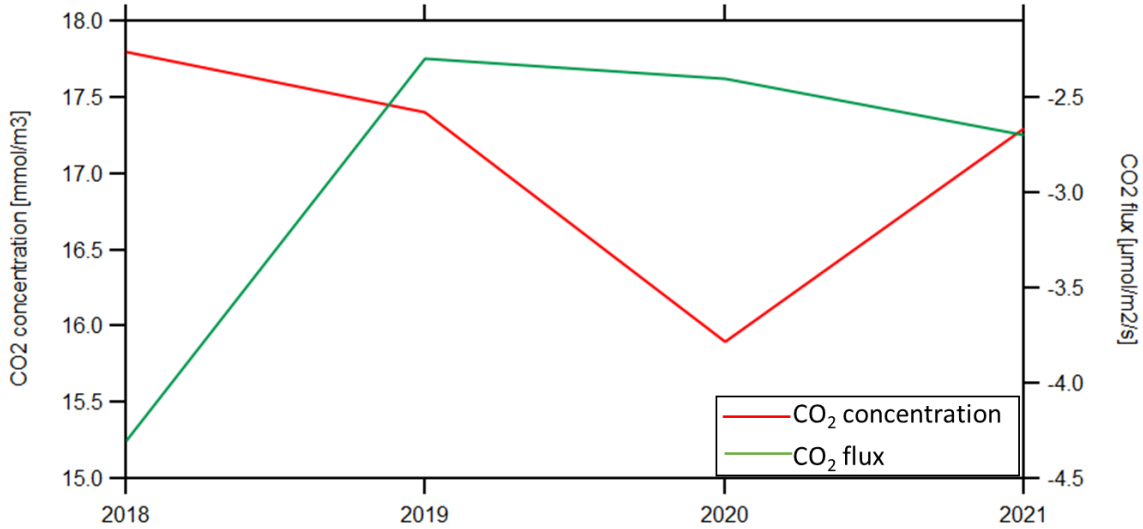


Figure 5.5: CO₂ concentration (red lines) compared with CO₂ flux (green line) of 15 days in March/April of each year from 2018 to 2021. (Added a legend to the image)

5.2 Comparison of the CO₂ flux calculated by the CLM5.0 model and the CO₂ flux of this project.

In this project, the average value of CO₂ flux in March/April was -4.3 µmol/m²/s in 2018, -2.3 µmol/m²/s in 2019, -2.4 µmol/m²/s in 2020, and -2.7 µmol/m²/s in 2021. The CO₂ flux calculated by CLM5.0 is -16 µmol/m²/s when temperature is 20° and humidity is 50% (for an assumed net photosynthesis of $A_n = 10$ µmol/m²/s). When T= -6.3° and RH=50%, the CO₂ flux value calculated by CLM5.0 mode is -17.7 µmol/m²/s. When T= 5.1° and RH=50%, the CO₂ flux value calculated by CLM5.0 mode is -16.9 µmol/m²/s. This shows that under the same temperature (-6.3° in 2018 and 5.1° in 2021), the CO₂ absorbed by the forest at the YAJP site is less than that calculated by the CLM5.0 model. The reason for this gap could be the difference in environmental conditions. The CO₂ flux measured by this project is in March/April of each year. At this time, it is spring and the temperature is low, generally below zero (-6.3° in 2018, -0.4° in 2019, and 2020 was -3.6°) or relatively low (5.1° in 2021). The content of water vapour in the air is also low. Therefore, the forest absorbs less CO₂. Our calculations with the CLM5.0 model assumes that the sky is clear, the temperature is 20°, and the humidity is 50%. Under this condition, CLM5.0 model will

predict more CO₂ absorption than under the weather conditions of this project. However, at the YAJP site in March and April, the temperature is lower than 20°, generally between -12° and 19° (according to the temperature data of 2021). When the temperature is 19° (the highest temperature from March 26 to April 10, 2021), the CO₂ flux of the YAJP site is -10.3 μmol/m²/s. Therefore, the calculated CO₂ flux results under the two conditions are different.

Comparing the CO₂ flux -16 μmol/m²/s measured by the CLM5.0 model under warm conditions with the CO₂ flux -22.9 μmol/m²/s measured by the YAJP tower under the same warm conditions (e.g., noon in the summer of August 25, 2021, T=20°, shown in Figure 5.7), we find that the value measured by the YAJP tower is larger in magnitude than the value modelled by CLM5.0. This indicates that the YAJP site absorbs more CO₂ from the forest that is predicted by the CLM5.0 model under warm environmental conditions.

5.3 Comparison of CO₂ concentration with other studies

The global CO₂ concentration changes from 2017 to 2022 are shown in Figure 5.6 (reproduced from the Global Monitoring Laboratory, GML). According to GML statistics, the whole year of global average concentration of CO₂ was 408 ppm in 2018, 410 ppm in 2019, and 412 ppm in 2020. The CO₂ concentration of the YAJP site was 389 ppm from September 2017 to September 2018, 408 ppm from April to September in 2019, 423 ppm from March to July in 2020, and 433 ppm from January to August in 2021. The reason for the averages over different range of dates was instrument failure and lost of data, so the measurement results are incomplete.

Figure 5.6 compares the monthly average CO₂ concentration measured at the YAJP tower with the global monthly average CO₂ concentration measured by GML. It can be seen that the CO₂ concentration measured at the YAJP site was much lower than the CO₂ concentration measured by GML. The first reason for this gap could be because the YAJP site is far away from urban areas and there is no CO₂ emissions from urban areas, and the

YAJP site is a pure coniferous forest with a single composition, so there are fewer conditions that affect the plant's absorption and release of CO₂. The second reason is because there are forests near the YAJP site. Although the site is close to the oil sands processing facility, the forest absorbs CO₂ from the atmosphere. The global monthly average CO₂ concentration summarized by GML was the sum of all various environments, such as cities, forests, and plains. Therefore, the CO₂ concentration in the atmosphere at the YAJP forest site is lower than the global CO₂ average measured by GML.

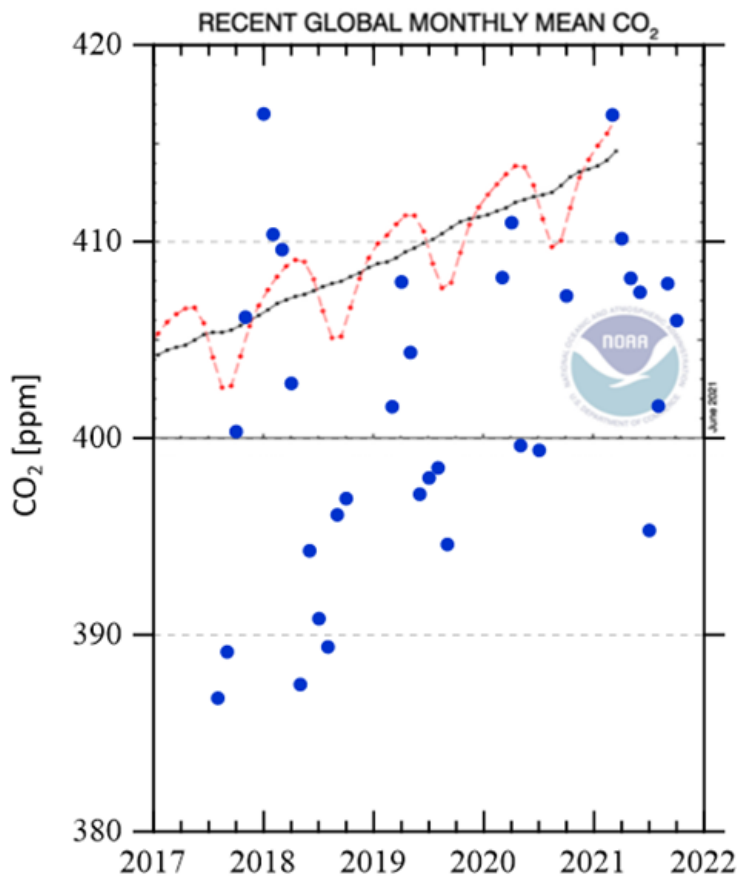


Figure 5.6: Comparison of monthly average CO₂ concentration measured by YAJP tower and global monthly mean CO₂ concentration measured by Global Monitoring Laboratory (GML).

5.4 Comparisons of CO₂ flux with other studies

Different forest components also have different uptake and release of CO₂, as shown in Table 2. Froelich et al. (2015) researched and collected 17 years (1996 to 2013) of data at the Borden Forest and they concluded that the forest is a low-to-medium sink of carbon with an average uptake of 177 g C/m²/y (NEP). At the YAJP site studied for this project, the average uptake CO₂ flux at 31 meters is about 99 g C/m²/y from September 2017 to September 2018 (calculated for this full year since this is the most complete continuous time series). The difference in CO₂ flux between Borden Forest and YAJP forest is due to differences in the composition of the two forests. The Borden Forest is a mixed forest, including *Acer rubrum*, Black Spruce, and Jack Pine. But the YAJP Forest is a pure coniferous forest. On the other hand, the trees in the Borden Forest have denser leaves, with a leaf area index (LAI) of 4 (Gordon et al. 2011), but the LAI of the YAJP forest is about 2. the higher the plant's LAI, the more carbon dioxide the plant absorbs (Juurola, 2016 and Eq. 16). For example, using the CLM5 model, when the given conditions are constant, the temperature is 20° and the humidity is 50%, when LAI=2, the CO₂ flux is -16.1 μmol/m²/s, and when LAI=4, the CO₂ flux is -32.1 μmol/m²/s.

The YAJP location is compared with other Canadian boreal forests, such as the boreal forests of Chibougamau, the boreal forests of Saskatchewan, and Manitoba. These boreal forests are dominated by black spruce, only Saskatchewan has a small amount of jack pine, and the YAJP research site is pure jack pine forest. The jack pine forest is not only different from black spruce forest in LAI, but also has a different canopy height. The black spruce site is about 10 m (Bergeron, 2007), while the jack pine on YAJP site is 19-22 m.

As shown in Figure 5.7, in the summer, the CO₂ flux from the YAJP forest is negative during the day, indicating that CO₂ is absorbed by vegetation. The CO₂ flux is positive at night, which indicates that vegetation is respiring. And comparing the boreal forests of other countries, in the same summer, the daytime CO₂ flux of Hyttiälä Forest is negative, and the nighttime CO₂ flux is greater than zero (Figure 2.6), which shows that CO₂ flux in

the Hyytiälä Forest at night is positive, and CO₂ is released. However, the daytime CO₂ flux values at the YAJP site were larger than the daytime CO₂ flux at Hyytiälä forest. The reason for this difference is that the two forests have different types of trees and the geographical locations of the two forests are also different.

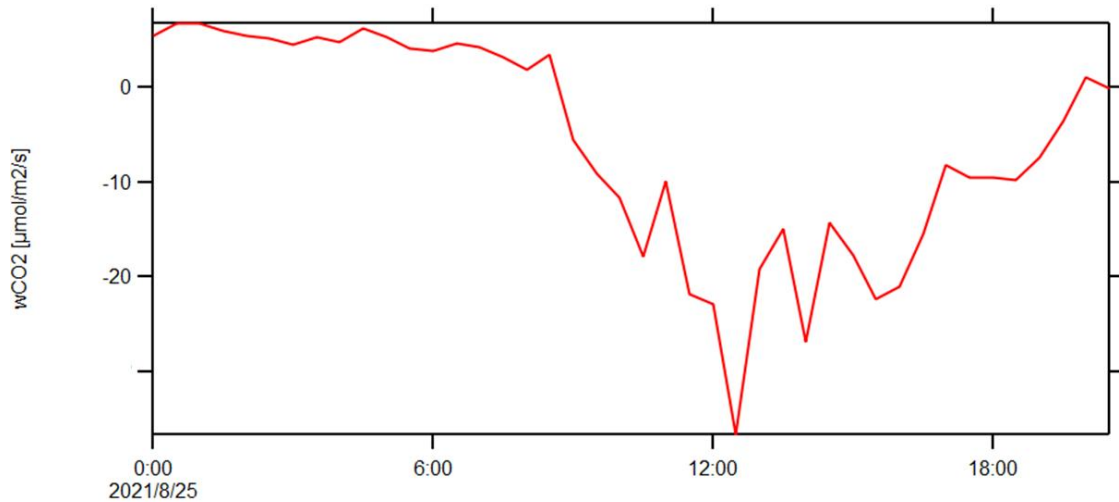


Figure 5.7: CO₂ flux measured at the YAJP tower in Aug.25th, 2021.

There are many conditions that affect the photosynthesis of trees. In addition to light, temperature and moisture, there are also conditions such as soil moisture, soil temperature, and plant stomata. Moreover, trees are much higher than ground plants, so the CO₂ flux at high places is easily affected by the weather and turbulence.

In British Columbia, the CO₂ flux of forests dominated by moss and lichens (-2.7 µmol/m²/s) is smaller than YAJP site which dominated by trees (-4.3 µmol/m²/s in 2018), because compared to trees, moss and lichens absorb less CO₂ and are less affected by light, temperature and water vapour.

For the impact of fire on forest CO₂ exchange, the temporal and spatial variation of fire frequency in YAJP forest (the Canadian boreal forest) is based on stand age. Jack pine forests and aspen forests have higher fire frequency than black spruce forests and white spruce forests (Köster, 2018). These changes in fire frequency may be related to the surrounding average water distribution (Larsen, 1997). The northern forests of Siberia are

located at high latitudes, the surface form is dominated by permafrost near melting, and the ecosystem is more susceptible to climate change. The increase in the depth of the active layer that melts during the northern forest season here may increase the soil temperature, which reduces the water in the soil and increase the CO₂ emissions (Köster, 2018). This may lead to higher CO₂ emissions from Siberian boreal forests than YAJP forests.

Table 2: Net ecosystem production (NEP) in different forest.

Site	Forest type	CO₂ flux
EOBS	Old Black Spruce	4±8 g C/m ² /yr
SOBS	Old Black Spruce	30±5 g C/m ² /yr
NOBS	Old Black Spruce	27±11 g C/m ² /yr
YAJP	Jack Pine	99 g C/m ² /yr
Borden forest	Mixed forest	177 g C/m ² /yr
Chibougamau, Quebec	Black Spruce	175 g C/m ² /yr
Northern Sweden	Pruce-Pine forest	261 g C/m ² /yr

6. Conclusion

According to the research results, the correlation between photosynthetically active radiation (PAR) and CO₂ flux was the highest, with a correlation of R=-0.9. Therefore, CO₂ flux is mainly driven by photosynthesis. Temperature and water vapour also affect CO₂ exchanges. When the temperature and water vapor content increased, plant photosynthesis was enhanced, so the CO₂ concentration in the air decreased. The degree of correlation between temperature and CO₂ concentration is R=0.07, and the degree of correlation between water vapour concentration and CO₂ concentration is R=-0.08. The degree of correlation between temperature and CO₂ flux is R=0.5, and the degree of correlation between water vapour concentration and CO₂ flux is R=0.8. But too high temperature and too much water vapour can reduce the photosynthesis of plants. As shown in Figure 4.2 and Figure 4.3, because the temperature is lower in March and April, the metabolism of plants is slower than in summer. CO₂ absorbed in spring is less than in summer

The temperature increased from March/April 2018 to March/April 2019, and decreased March/April 2019 to March/April 2020, then increased again in 2021. The H₂O flux in the atmosphere showed a slow growth trend during March/April from 2018 to 2020, but in 2021, it has increased slightly. The CO₂ concentration at the YAJP site declined in March/April 2018 to 2020, however, in 2021 the average value has increased.

The average value of CO₂ flux in March/April was -4.3 μmol/m²/s in 2018, -2.3 μmol/m²/s in 2019, -2.4 μmol/m²/s in 2020, and -2.7 μmol/m²/s in 2021. The CO₂ flux of the YAJP site was -15.5 μmol/m²/s from September 2017 to September 2018, -15.8 μmol/m²/s from April to September in 2019, -16.6 μmol/m²/s from March to July in 2020, and -16.8 μmol/m²/s from January to August in 2021. The forest at this research area is a sink of carbon.

The forest in the YAJP study area is close to the oil sands production facilities. These facilities release a large number of pollutants, affecting the CO₂ flux of the forest. The wind direction from 170° to 190° brings higher SO₂ (averages of 3.4 to 3.8 ppb) to the YAJP

tower, indicating that pollutants detected by the tower generally appear to come from Suncor facilities. We also see higher CO₂ concentration (17.2 to 17.3 mmol/m³) from this direction and higher CO₂ fluxes (-5.5 μmol/m²/s), indicating that the pollution levels may be related to CO₂ uptake by the forest. When the wind directions are outside this range, the CO₂ concentration is 16.8 mmol/m³ and the CO₂ flux is -3.4 μmol/m²/s.

References

- Adams, E. E. (2012). World Forest Area Still on the Decline. Earth Policy Institute
http://www.earthpolicy.org/indicators/C56/forests_2012
- "Alberta Energy: Facts and Statistics". Alberta Energy. Archived from the original on 2017-05-28. Retrieved 2014-04-19.
- "Alberta's Oil Sands 2006" (PDF). Government of Alberta. 2007. Archived from the original (PDF) on 2008-02-27. Retrieved 2008-02-17.
- Bao, J. W., Michelson, S. A., Persson, P. O. G., Djalalova, I. V., & Wilczak, J. M. (2008). Observed and WRF-Simulated Low-Level Winds in a High-Ozone Episode during the Central California Ozone Study. *Journal of Applied Meteorology and Climatology*, 47(9), 2372–2394. <https://doi.org/10.1175/2008JAMC1822.1>
- Baldocchi. (2003). Assessing the eddy covariance technique for evaluating carbon dioxide exchange rates of ecosystems: past, present and future. *Global Change Biology*, 9(4), 479–492. <https://doi.org/10.1046/j.1365-2486.2003.00629.x>
- Bergeron, O., Margolis, H. A., Black, T. A., Coursolle, C., Dunn, A. L., Barr, A. G., & Wofsy, S. C. (2007). Comparison of carbon dioxide fluxes over three boreal black spruce forests in Canada. *Global Change Biology*, 13(1), 89–107.
<https://doi.org/10.1111/j.1365-2486.2006.01281.x>
- Beecken, J., Mellqvist, J., Salo, K., Ekholm, J., & Jalkanen, J. P. (2014). Airborne emission measurements of SO₂, NO_x and particles from individual ships using a sniffer technique. *Atmospheric Measurement Techniques*, 7(7), 1957. https://link.gale.com/apps/doc/A481418335/AONE?u=yorku_main&sid=bookmark-AONE&xid=60fb8e91
- Botting, R. S., & Fredeen, A. L. (2006). Net ecosystem CO₂ exchange for moss and lichen dominated forest floors of old-growth sub-boreal spruce forests in central British Columbia, Canada. *Forest Ecology and Management*, 235(1–3), 240–251.
<https://doi.org/10.1016/j.foreco.2006.08.332>

- Brandt, J.P., Flannigan, M.D., Maynard, D.G., Thompson, I.D., and Volney, W.J.A. 2013. An introduction to Canada's boreal zone: ecosystem processes, health, sustainability, and environmental issues. *Environ. Rev.* This issue. doi:10.1139/er-2013-0040.
- Burba, G., (Lead Author) Catherine, G. (Topic Editor). 2008. "Flux footprint." In: *Encyclopedia of Earth*. Eds. Cutler J. Cleveland (Washington, D.C.: Environmental Information Coalition, National Council for Science and the Environment).
- CAPP (2018). *Canada's Oil Sands Report*. Canada's Oil and Natural Gas Producers.
- Chi, J. S., Zhao, P., Klosterhalfen, A., Jocher, G., Kljun, N., Nilsson, M. B., & Peichl, M. (2021). Forest floor fluxes drive differences in the carbon balance of contrasting boreal forest stands. *Agricultural and Forest Meteorology*, 306, 108454–. <https://doi.org/10.1016/j.agrformet.2021.108454>
- Community Earth System Model (CESM). 2021.
- David, M., Martin S. (November 2008). *Canadian Oil Sands Supply Costs and Development Projects*. Canadian Energy Research Institute. ISBN 978-1-896091-83-9.
- Dennis D. Baldocchi, Christoph A. Vogel, Brad Hall. 1995. Seasonal variation of carbon dioxide exchange rates above and below a boreal jack pine forest. *Agricultural and Forest Meteorology* 83 (1997) 147- 170.
- (ECCC 2016) Environment and Climate Change Canada, & Alberta Environment and Parks (2016). *Joint Oil Sands Monitoring Program Emissions Inventory Compilation Report*. Edmonton: Her Majesty the Queen in right of the Province of Alberta.
- Eija Juurola et al.(2016), Carbon tree. date of last access Is 2017. <http://hiilipuu.fi/articles/forests>
- FAO. 2010. *Global Forest Resources Assessment 2010*. Food and Agricultural Organization of the United Nations, Rome. Forestry Paper 163.
- Foken, T. (2017). *Micrometeorology*. Springer Berlin Heidelberg.

- Froelich, N., Croft, H., Chen, J. M., Gonsamo, A., & Staebler, R. M. (2015). Trends of carbon fluxes and climate over a mixed temperate–boreal transition forest in southern Ontario, Canada. *Agricultural and Forest Meteorology*, 211–212(Complete), 72–84. <https://doi.org/10.1016/j.agrformet.2015.05.009>
- Gardner, Timothy (2009-05-18). "Canada oil sands emit more CO₂ than average: report". Reuters. Archived from the original on 2012-03-29. Retrieved 2011-08-27.
- Gao, Avramov, A., Saikawa, E., & Schlosser, C. A. (2021). Emulation of Community Land Model Version 5 (CLM5) to Quantify Sensitivity of Soil Moisture to Uncertain Parameters. *Journal of Hydrometeorology*, 22(2), 259–278. <https://doi.org/10.1175/JHM-D-20-0043.1>.
- Giasson, M. A., Coursolle, C., & Margolis, H. A. (2006). Ecosystem-level CO₂ fluxes from a boreal cutover in eastern Canada before and after scarification. *Agricultural and Forest Meteorology*, 140(1-4), 23–40. <https://doi.org/10.1016/j.agrformet.2006.08.001>
- Gordon, M. et al. (2011). Aerosol flux measurements above a mixed forest at Borden, Ontario. *Atmos. Chem. Phys.*, 11, 6773-6786.
- Global Monitoring Laboratory (2021). Recent global monthly mean CO₂ concentration
- Hayes, D.J., Turner, D.P., Stinson, G., McGuire, A.D., Wei, Y., West, T.O., Heath, L.S., Jong, B., McConkey, B.G., Birdsey, R.A., Kurz, W.A., Jacobson, A.R., Huntzinger, D.N., Pan, Y., Post, W.M., and Cook, R.B. 2012. Reconciling estimates of the contemporary North American carbon balance among terrestrial biosphere models, atmospheric inversions, and a new approach for estimating net ecosystem exchange from inventory-based data. *GlobalChange Biol.* 18(4): 1282–1299. doi:10.1111/j.1365-2486.2011.02627.x.
- Helbig, M., Chasmer, L. E., Desai, A. R., Kljun, N., Quinton, W. L., & Sonnentag, O. (2017). Direct and indirect climate change effects on carbon dioxide fluxes in a thawing boreal forest–wetland landscape. *Global Change Biology*, 23(8), 3231–3248.

<https://doi.org/10.1111/gcb.13638>

- Hollinger, D. Y., Goltz, S. M., Davidson, E. A., Lee, J. T., Tu, K., & Valentine, H. T. (1999). Seasonal patterns and environmental control of carbon dioxide and water vapour exchange in an ecotonal boreal forest. *Global Change Biology*, 5(8), 891–902. <https://doi.org/10.1046/j.1365-2486.1999.00281.x>
- Huntzinger, D.N., Post, W.M., Wei, Y., Michalak, A.M., West, T.O., Jacobson, A.R., Baker, I.T., Chen, J.M., Davis, K.J., Hayes, D.J., Hoffman, F.M., Jain, A.KMcGuire, A.D., Neilson, R.P., Potter, Chris, Poulter, B., Price, David, Raczka, B.M., Tian, H.Q., Thornton, P., Tomelleri, E., Viovy, N., Xiao, J., Yuan, W., Zeng, N., Zhao, M., and Cook, R. 2012. North American Carbon Project (NACP) regional interim synthesis: terrestrial biospheric model intercomparison. *Ecol. Model.* 232: 144–157. [doi:10.1016/j.ecolmodel.2012.02.004](https://doi.org/10.1016/j.ecolmodel.2012.02.004).
- Thornley. (1998). Dynamic Model of Leaf Photosynthesis with Acclimation to Light and Nitrogen. *Annals of Botany*, 81(3), 421–430. <https://doi.org/10.1006/anbo.1997.0575>
- Jiang, K. (2018). Mixing and Deposition in a Jack Pine Forest Canopy. Graduate program in Earth and Space Science, York University Toronto, Ontario.
- Kurz, W. ., Shaw, C. ., Boisvenue, C., Stinson, G., Metsaranta, J., Leckie, D., Dyk, A., Smyth, C., & Neilson, E. . (2013). Carbon in Canada’s boreal forest — A synthesis. *Environmental Reviews*, 21(4), 260–292. <https://doi.org/10.1139/er-2013-0041>
- Kaimal, J. C., Finnican, J.J. (1994). *Atmospheric Boundary Layer Flows*. Oxford University Press.
- Köster, E., Köster, K., Berninger, F., Prokushkin, A., Aaltonen, H., Zhou, X., & Pumpanen, J. (2018). Changes in fluxes of carbon dioxide and methane caused by fire in Siberian boreal forest with continuous permafrost. *Journal of Environmental Management*, 228(Complete), 405–415. <https://doi.org/10.1016/j.jenvman.2018.09.051>.
- Kljun, Calanca, P., Rotach, M. W., & Schmid, H. P. (2004). A Simple Parameterisation for

Flux Footprint Predictions. *Boundary-Layer Meteorology*, 112(3), 503–523.

<https://doi.org/10.1023/B:BOUN.0000030653.71031.96>

- Luysaert, S., Inghima, I., Jung, M., Richardson, A. D., Reichstein, M., Papale, D., Piao, S. L., Schulze, E.-D., Wingate, L., Matteucci, G., Aragao, L., Aubinet, M., Beer, C., Bernhofer, C., Black, K. G., Bonal, D., Bonnefond, J.-M., Chambers, J., Ciais, P., Gielen, B. (2007). CO₂ balance of boreal, temperate, and tropical forests derived from a global database. *Global Change Biology*, 13(12), 2509–2537.
- Margolis, H. A., & Ryan, M. G. (1997). A physiological basis for biosphere-atmosphere interactions in the boreal forest: an overview. *Tree Physiology*, 17(8–9), 491–499.
<https://doi.org/10.1093/treephys/17.8-9.491>.
- Marshall, & Biscoe, P. V. (1980). A Model for C₃ Leaves Describing the Dependence of Net Photosynthesis on Irradiance. *Journal of Experimental Botany*, 31(1), 29–39.
<https://doi.org/10.1093/jxb/31.1.29>.
- Mammarella, Kolari, P., Rinne, J., Keronen, P., Pumpanen, J., & Vesala, T. (2007). Determining the contribution of vertical advection to the net ecosystem exchange at Hyytiälä forest, Finland. *Tellus. Series B, Chemical and Physical Meteorology*, 59(5). <https://doi.org/10.3402/tellusb.v59i5.17068>
- Medlyn, B.E., Duursma, R.A., Eamus, D., Ellsworth, D.S., Prentice, I.C., Barton, C.V.M., Crous, K.Y., De Angelis, P., Freeman, M., and Wingate, L., 2011. Reconciling the optimal and empirical approaches to modelling stomatal conductance. *Global Change Biology*, 17: 2134–2144. doi:10.1111/j.1365-2486.2010.02375.x
- Miles, N., Davis, K., Richardson, S., Lauvaux, T., Martins, D., Deng, A., Balashov, N., Gurney, K., Liang, J., Roest, G., Wang, J., & Turnbull, J. (2021). The influence of near-field fluxes on seasonal carbon dioxide enhancements: results from the Indianapolis Flux Experiment (INFLUX). *Carbon Balance and Management*, 16(1), 4–4. <https://doi.org/10.1186/s13021-020-00166-z>

- Pertti Hari, Kari Heliövaara, Liisa Kulmala (2012), Physical and Physiological Forest Ecology. <https://www.springer.com/gp/book/9789400756021>
- Pregitzer, K. S., & Euskirchen, E. S. (2004). Carbon cycling and storage in world forests: biome patterns related to forest age. *Global Change Biology*, 10(12), 2052–2077. <https://doi.org/10.1111/j.1365-2486.2004.00866.x>
- Ruimy, A., Jarvis, P.G., Baldocchi, D.D. and Saugier, B., 1995. CO₂ Fluxes over plant canopies and solar radiation: a literature review. *Adv. Ecol. Res.*, 26: 1-68.
- Seinfeld, & Pandis, S. N. (1998). Atmospheric chemistry and physics : from air pollution to climate change . Wiley.
- Sun, W., Kooijmans, L. M. J., Maseyk, K., Chen, H., Mammarella, I., Vesala, T., Levula, J., Keskinen, H., & Seibt, U. (2018). Soil fluxes of carbonyl sulfide (COS), carbon monoxide, and carbon dioxide in a boreal forest in southern Finland. *Atmospheric Chemistry and Physics*, 18(2), 1363–1378. <https://doi.org/10.5194/acp-18-1363-2018>.
- Wood Buffalo Environmental Association. (2019). JP104: Monitoring Stations. Retrieved from <https://wbea.org/towers/jp104/>.
- Yvon-Durocher, Caffrey, J. M., Woodward, G., Allen, A. P., Cescatti, A., Dossena, M., Del Giorgio, P., Gasol, J. M., Montoya, J. M., Pumpanen, J., Staehr, P. A., & Trimmer, M. (2012). Reconciling the temperature dependence of respiration across timescales and ecosystem types. *Nature (London)*, 487(7408), 472–476. <https://doi.org/10.1038/nature11205>